MEDWIN PUBLISHERS
Committed to create value for Researchers

Physical Science & Biophysics Journal

Entanglement-Enabled Information Processing Implies Human Consciousness Mechanism

W Grant Cooper*

International Physics Health & Energy, Texas Tech University College of Education, USA

Conceptual Paper

Volume 2 Issue 1

Received Date: March 22, 2018

Published Date: May 09, 2018

***Corresponding author:** W Grant Cooper, International Physics Health & Energy, Texas Tech University College of Education, Lubbock, USA, Tel: 1-8067625322; Email: cooperwg@sbcglobal.net

Abstract

Quantum information processing of EPR-generated entangled proton qubits exhibited by rat and human genomes falsifies the *in vivo* anti-entanglement hypothesis. An EPR-entangled proton qubit algorithm explains "probabilistic" genomic growth — over the past ~ $3.6\text{x}10^9$ y — from primordial duplex RNA–ribozyme segments, into a DNA double helix of ~ $6.8\text{x}10^9$ bp. *Homo sapiens'* consciousness is thus considered a consequence of ~$3.6\text{x}10^9$ y of entanglement-enabled evolution. The evolved human brain acquired sensory "biological files" for vision, acoustics, vocal, olfactory, touch, taste, balance, self-motion, pain, emotion, language, analytical, music, imagination, "truth" and "fantasy". Sensory files are interfaced with, initially vacant, "hard drive" memory files that acquire input data from one or all sensory files. Each "new" experience (stimulus) generates input for "hard drive" memory. This stimulus creates an entanglement state between the "measured", entangled groove-proton "qubit-pair" and Grover's enzyme quantum processor, which executes quantum information processing, $\Delta t' \leq 10^{-14}$ s, *before* proton decoherence, $\tau_D < 10^{-13}$ s. The sequence of acquired input events, e.g., successfully riding a bicycle, is "permanently" stored. When EPR-generated entangled proton qubit-pairs populate DNA sequences *not* evolutionarily selected for normal quantum information processing in neurological cells, heritable neurological diseases — e.g., Huntington's disease and congenital myotonic dystrophy — are exhibited, thereby protecting the gene pool against evolutionary extinction. Anesthetics inhibit Grover's quantum-reader enzyme from quantifying quantum informational content within EPR-generated entangled proton qubits. This absence of quantum information processing instructions disallows normal consciousness, yielding unconsciousness. Significance of entanglement is illustrated by age-related cancer data (ages 10 to 80 y). "Accurate" evaluation by a "corrected" Muller's constant "mutational load" expression, i.e., $dN/dt = \lambda + \beta t$ – where βt ($\beta \approx 2.2\text{x}10^{-23}$ s^{-2}) is an EPR-entanglement term – yields assessments that clearly identify EPR-entanglement terms, $\Sigma_j \beta_j t^4$, as *solely* responsible for age-related cancer manifestation, but classical contributions – $\Sigma i \lambda i t^3$, "passenger mutations" – do *not* contribute to disease.

Keywords: Anti-entanglement hypothesis falsification; Brain-cell quantum processing; Classical–quantum interface; Entangled qubits' consciousness model; Entangled "qubit-pair" measurement uncertainty; Entanglement-selected genetic code origin; EPR-proton qubits; Grover's algorithm; Löwdin's hypothesis; Quantum information processing

Introduction

Fundamental physics and biology questions currently asked of molecular bio-science include: What "microscopic" molecular mechanisms are responsible for (***a***) origin of *sustainable* life on prebiotic Earth and (***b***) origin and existence of human brain consciousness? The purpose of this report is to present evidence that a plausible model for human consciousness can be constructed in terms of an extrapolation, over the past ~ $3.6x10^9$ y, of EPR-generated entangled proton qubits, subjected to entanglement-enabled information processing evolution [1-2]. Grover's-type quantum processor measurements, $\delta t << 10^{-13}$ s of EPR-generated entangled proton qubit-pairs specify evolutionary distributions of rat and human microsatellites [1,16-21]. Since the evolutionary "emergence-distance" between rat and human is ~ $70x10^6$ y, EPR-generated entangled proton qubit-pairs *must retain* entangled "two-state" quantum coherence, $|+> \rightleftarrows |->$, *for years to decades*, before specifying microsatellite evolution instructions with "measured" quantum informational content of EPR-generated entangled proton qubit-pairs [17-19,22]. Otherwise, Grover's-type quantum processor measurements, $\delta t << 10^{-13}$ s, of EPR-generated entangled proton qubit-pairs could *not* accurately specify evolutionary distributions of the 22 most abundant microsatellites common to rat and human, as exhibited [10-12,16-18,20,21]. Consequently, reduced energy, EPR-generated entangled proton qubit-pairs participate in entangled quantum oscillations, ~ $4x10^{13}$ s–1, between indistinguishable sets of electron lone-pairs within decoherence-free subspaces of enol oxygen and imine nitrogen, on opposite genome strands (Figures 1-4) — *for years to decades*— before "measured by" Grover's quantum reader-processor [1,10-12,16-20,23-25].

Amino protons encounter quantum uncertainty limits, $\Delta x \Delta p_x \geq \hbar/2$, introducing probabilities of EPR arrangements, *keto-amino —(entanglement)→ enol–imine.* The asymmetric double-well potential represents an energy surface "seen by" a metastable hydrogen bonding amino proton, and a "ground state", entangled enol and imine proton "qubit-pair". Product enol and imine protons are entangled, and are each shared between two indistinguishable sets of electron lone-pairs, and thus, participate in entangled quantum oscillations, $|+> \rightleftarrows |->$, between near symmetric energy wells, occupying *intramolecular* decoherence-free subspaces.

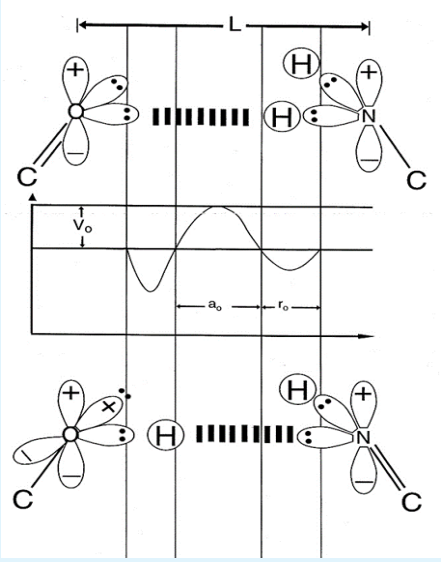

Figure 1: Schematic of "metastable" keto-amino and "ground state" enol-imine hydrogen bonds.

The anti-entanglement hypothesis asserts that entangled superposition quantum states occupying ~ 37°C, *in vivo* environments encounter decoherence before entangled coherent states could functionally contribute quantum enhancements to susceptible reactive biological processes; so, quantum entanglement phenomena do not significantly contribute to *in vivo* biological processes [26-31]. This hypothesis is falsified by Grover's-type [20] measurements of EPR-generated, entangled proton qubit-pairs, which specify entanglement-enabled information processing and evolution of rat and human microsatellites [16-21]. In these cases, metastable hydrogen bonded amino ($-NH_2$) genome protons encounter quantum uncertainty limits, $\Delta x\ \Delta p_x \geq \hbar/2$ [32-33]. The resulting quantum mechanical proton – proton interaction introduces probabilities of EPR-arrangements, *keto-amino*

—*(entanglement)* → *enol-imine*, yielding "qubit-pairs" of entangled enol and imine protons [1-2,16]. EPR-generated entangled proton qubit-pairs, $|+\rangle \rightleftarrows |-\rangle$, occupy decoherence-free subspaces — between two different indistinguishable sets of electron lone-pairs — for years to decades, before a Grover's [20] processor transcriptase measurement of an entangled "qubit-pair" specifies evolution instructions for human and/or rat microsatellites [10-12,16-21,23-25]. Based on recent studies Grover's [20] processors measure quantum informational content embedded within EPR-generated entangled proton qubits [16-19]. This measurement of quantum informational content (entangled proton qubit-pairs) specifies instructions for subsequent quantum information processing, which governs time-dependent evolution [17-18,21]. Within this context, this report presents an argument that human consciousness is a consequence of ~ 3.6×10^{9} y of entanglement-enabled information processing evolution [1-2,6-9,10-19].

This report reviews evidence that EPR-generated entangled proton qubit-pairs are "measured by", $\delta t << 10^{-13}$ s, Grover's [20] processors, which specify quantum information processing instructions, $\Delta t' \leq 10^{-14}$ s, exhibited by prokaryotic (T4 phage) and eukaryotic (rat and human) genomic systems [10-12,16-19,35,36]. Since evolutionarily selected quantum information processing is clearly exhibited by human genomes, this entanglement-enabled information processing potential resides within human brain-cell DNA, and consequently, is available to implement analogous quantum information processing to expedite cognitive processes responsible for consciousness [6-9,18]. The following six sections convey this message. Section II outlines the creation of EPR-generated entangled proton qubits, and measurement of corresponding quantum informational content by Grover's processors [20], which specifies quantum information processing instructions. A quantum mechanical model for origin of the genetic code – 4^3 codons for ~ 22 L-amino acids – is presented in Section III. The next section illustrates a method for correcting erroneous, "classical-only" representations of time-dependent molecular genomic reactive processes, by *not* neglecting "proper" quantum entanglement, EPR-contributions. This is accomplished by adding an approximate quantum entanglement term, βt – from EPR-entangled proton qubits' contribution – to Muller's constant "mutational load", yielding $dN/dt = \lambda + \beta t$. Enigmatic observations – age-related incidence of cancer (ages 10 to 80 y) – are then unambiguously described by, previously ignored, quantum entanglement terms, $\Sigma_j \beta_j t^4$, *exclusively*. Section V discusses implied roles of EPR-generated entangled proton qubits in *Homo sapiens*' brain-cell DNA cognitive processes that *could be* responsible for consciousness [6-9]. Section VI summarizes origins and biological consequences of EPR-generated entangled proton qubits. These include (***a***) entanglement-enabled origin of "sustainable" life in RNA, and subsequently, in DNA systems, (***b***) EPR-generated genomic growth via "dynamic mutation", and (***c***) species' survival in terms of "gatekeeper genes" quantifying magnitude of EPR-generated entangled proton qubits in *H. sapiens'* haploid and diploid genomic systems. Section VII concludes that EPR-generated entangled proton qubits have been an "unrecognized", but significant, participant in quantum information processing responsible for genomic evolution, and may be primary participants in executing quantum information processing by brain-cell DNA, required for consciousness. The Appendix presents a three-level quantum approximation for obtaining an approximate "rate constant", $\beta = (\gamma_\rho/\hbar)^2 \approx 2\times10^{-23}\ s^{-2}$ (WG Cooper, unpublished result), for EPR-generated entangled proton qubit arrangements, *keto-amino* → *enol–imine*.

Entanglement-Enabled Information Processing

Creation of Entangled Proton Qubits

Consistent with evolutionary design the replicase introduces complementary G-C and A-T pairs into metastable *keto-amino* states [1-6,35-36]. Quantum informational content within duplex DNA is a consequence of metastable, hydrogen bonded amino ($-NH_2$) protons encountering quantum uncertainty limits $\Delta x\ \Delta p_x \geq \hbar/2$ [1,2,16-19,32,33]. This introduces a probability of direct quantum mechanical proton – proton interaction, yielding EPR-arrangements *keto-amino* — *(entanglement)* → *enol–imine* (Figures 1-4), observed as G-C → ***G´-C´***, G-C → ****G-*C*** and A-T → ****A-*T***. (**Bold** *italics* — ***G´-C´***, ****G-*C***, ****A-*T*** — denote necessity of Hilbert space to describe dynamics of embedded entangled proton qubit-pairs; (Figures 1-4) Reduced energy product enol and imine protons occupying *heteroduplex heterozygote* sites — ***G´-C´***, ****G-*C***, ****A-*T*** — contain EPR-generated, entangled proton qubits, shared between two different indistinguishable sets of electron lone-pairs belonging to decoherence-free subspaces of enol oxygen and imine nitrogen on opposite genome strands (Figures 1-4) [10-19,23-25,34,35-37]. These EPR-generated proton "qubit-pairs" participate in entangled, two-state quantum oscillations, $|+\rangle \rightleftarrows |-\rangle$, at ~ $4\times10^{13}\ s^{-1}$ (~ 4800 m s^{-1}) between near symmetric energy wells in decoherence-free subspaces — for years to decades — until measured, $\delta t << 10^{-13}$ s, in a major (~ 22 Å) or minor (~ 12 Å)

genome groove [38] by evolutionarily selected Grover's [20] quantum readers [17-19,21,23-25].

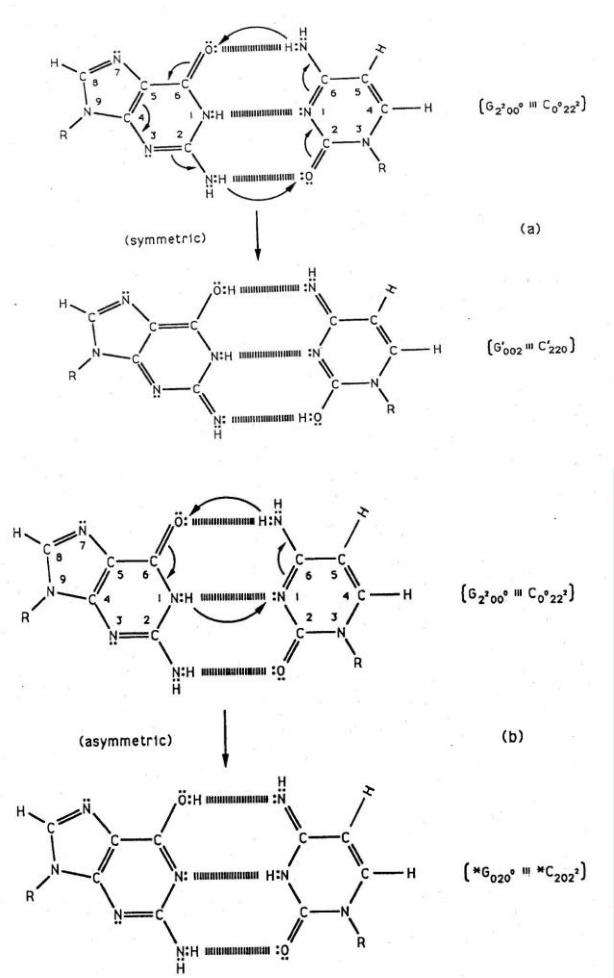

Figure 2: Symmetric (a) and asymmetric (b) channels for EPR-generated proton exchange — electron arrangement at a G-C site. a) Symmetric channel for proton exchange tunneling electron rearrangement, yielding two enol-imine hydrogen bonds between complementary G-C. Here an energetic guanine amino proton initiates the reaction. (b) The asymmetric exchange tunneling channel, yielding the G-C "hybrid state" containing one enol-imine and one keto-amino hydrogen bond. An energetic cytosine amino proton initiates reaction in this channel. An annulus of reaction is identified by arrows within each G-C reactant duplex. Electron lone-pairs are represented by double dots, :. Subscript notation for $^{*}G_{020}^{0}$, etc. is given in Figure 3 legend.

Before proton decoherence, $\tau_D < 10^{-13}$ s, proton – processor entanglement states implement quantum information processing, $\Delta t' \leq 10^{-14}$ s, including (i) transcription, (ii) translation, (iii) selection of accessible amino acids for peptide bond formation, (iv) initiation of genome growth and (v) random genetic drift [1-2,5,16,19,31,36]. This specifies peptide bond formation — ~ 8 to 16 KJ/mole from proton decoherence — and the final, decohered molecular clock state, which is an observable time-dependent substitution, *ts* — G′2 0 2 → T, G′0 0 2 → C, *G0 2 0^0 → A & *C2 0 2^2 → T — or deletion, td, *A → deletion & *T → deletion [5,16,35-36]. Entanglement-enabled substitutions, *ts*, are manifested as single nucleotide polymorphisms (*SNPs*), but are distinguishable from classically originated substitutions, SNPs [5,16,18]. (**Bold** *italics* distinguish entanglement-enabled *SNPs*, from classically originated SNPs). For example, *SNP* "driver" mutations originate via entanglement-enabled *ts*, but classical mechanisms introduce "passenger mutations", exhibited as SNPs [16,19].

An entangled enol or imine proton qubit is in state $|+>$ when it is in position to participate in interstrand hydrogen bonding (Figure 1) and is in state $|->$ when it is "outside", in a major or minor DNA groove [16-19,38]. The quantum mechanical state of the entangled pair of ***G-*C*** proton qubits can be viewed as a vector in the four-dimensional Hilbert space that describes the quantum position state of two protons. The most general quantum mechanical state of these two protons can be written as [39].

$$|\psi> = c{+}{+}|++> + c{+}{-}|+->+ c{-}{+}|-+> + c{-}{-}|--> \quad (1)$$

Where the first symbol, + or −, represents proton 1 and the second symbol represents proton 2, and the expansion coefficients, *c's,* satisfy normalization, $|c{+}{+}|^2 + |c{+}{-}|^2 + |c{-}{+}|^2 + |c{-}{-}|^2 = 1$. Since Eq (1) cannot be expressed as a tensor product of protons 1 and 2, maximally entangled quantum states for the qubit-pair of imine and enol protons can be written in terms of the four Bell states [40-41], expressed as

$$|\Phi^{+}> = 1/\sqrt{2}\,\{|++> + |--\} \quad (2)$$
$$|\Phi^{-}> = 1/\sqrt{2}\,\{|++> - |--\} \quad (3)$$
$$|\varphi^{+}> = 1/\sqrt{2}\,\{|+-> + |-+\} \quad (4)$$
$$|\varphi^{-}> = 1/\sqrt{2}\,\{|+-> - |-+\} \quad (5)$$

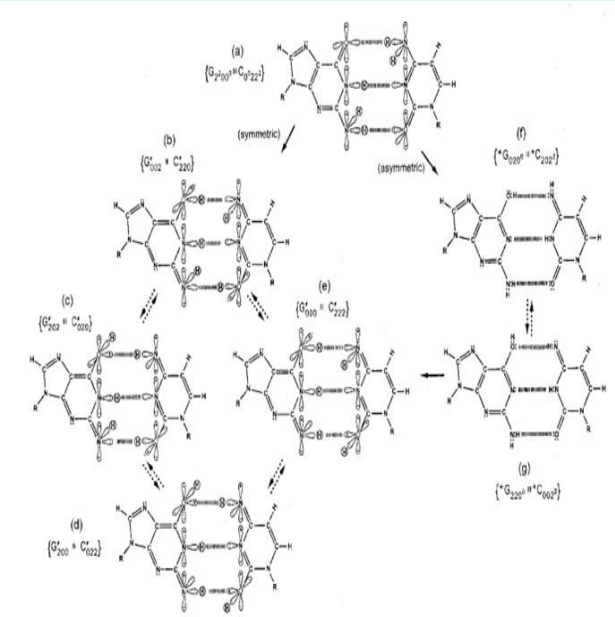

Figure 3: Distribution of entangled proton qubit states at a *G′-C′* (symmetric) or **G-*C* (asymmetric) superposition site. Symmetric, asymmetric and second asymmetric (unlabeled) channels (→) by which metastable keto-amino G-C protons populate enol and imine entangled proton qubit states. Dashed arrows identify pathways for quantum oscillation of enol and imine proton qubits. Approximate electronic structures for hydrogen bond end groups and corresponding proton positions are shown for the metastable keto-amino duplex (a) and for enol and imine entangled proton qubit states, *G′-C′* (b-e). Electron lone-pairs are represented by double dots, :, and a proton by a circled H. Proton states are specified by a compact notation, using letters G, C, A, T for DNA bases with 2's and 0's identifying electron lone-pairs and protons, respectively, donated to the hydrogen bond by – from left to right – the 6-carbon side chain, the ring nitrogen and the 2-carbon side chain. Superscripts identify the component at the outside position (in major and minor groves) as either an amino group proton, designated by 0^0, or a keto group electron lone-pair, indicated by 2^2. Superscripts are suppressed for enol and imine groups.)

electron lone-pairs, and thus, participates in entangled quantum oscillations between near symmetric energy wells at ~ 10^{13} s^{-1} in decoherence-free subspaces [23-25,40-45] which specifies entangled proton qubit informational-dynamics occupying a *heteroduplex heterozygote* ***G′-C′*** superposition site [16-19,35-37]. In this case, two sets of entangled imine and enol proton qubits — four protons constituting two sets of entangled "qubit-pairs" — occupy complementary ***G′-C′*** isomer super positions such that enzyme quantum reader "measurement" of ***G′***-protons specifies, instantaneously, quantum states of the four entangled qubits that occupy the sixteen-dimensional space [10-12].

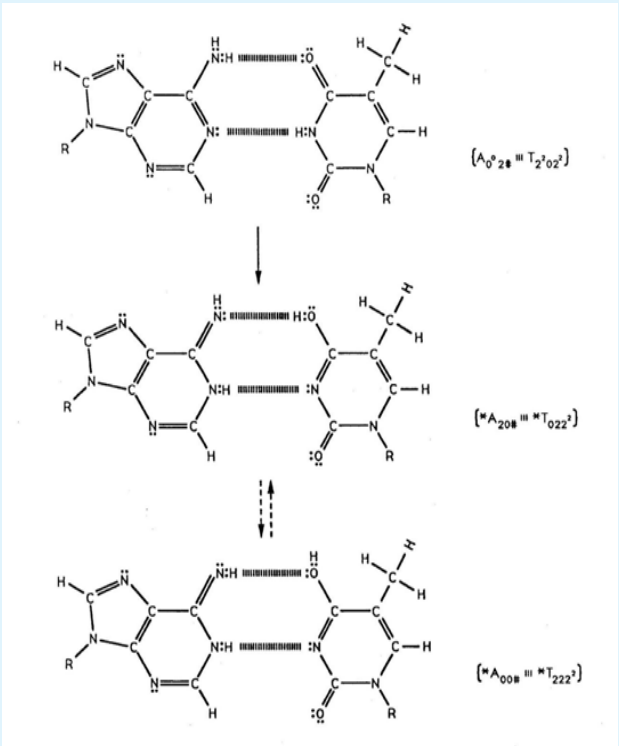

Figure 4: Pathway for metastable keto-amino A-T protons to populate enol and imine proton qubit states. Dashed arrows indicate proton oscillatory pathway for enol and imine proton qubit ***A-*T*** states Notation is given in Figure 3 legend. The # symbol indicates the position is occupied by ordinary hydrogen unsuitable for hydrogen bonding.

The dimensionality of the Hilbert space required to express the quantum mechanical state for four proton qubits occupying ***G′-C′*** isomer pair super positions is sixteen, i.e., $2^N = 2^4 = 16$. Each entangled imine and enol proton is shared between two sets of indistinguishable

Studies of *heteroduplex heterozygote* ***G′-C′*** sites, with ***G′*** on the transcribed strand, require the enzyme quantum reader to "measure", specify and execute quantum informational content of sixteen different entangled proton qubit ***G′-C′*** states (Table 1) [16-19]. In the case of

Fig. 5, ***G′0 0 2*** (***G′0 0 2 → C,*** Table 1) the carbon-2 imine proton is in state $|-\rangle$ "groove position", whereas the eigenstate ***G′2 0 2*** (***G′2 0 2 → T,*** Table 1) has both carbon-2 imine and carbon-6 enol protons in state $|-\rangle$ "groove positions". Eigenstate ***G′2 0 0*** (***G′2 0 0 → G***; "null" mutation) has the carbon-6 enol proton "trapped" in a state $|-\rangle$ DNA groove, but entangled enol and imine protons for eigenstate ***G′0 0 0*** are both in state $|+\rangle$, the "interior" interstrand hydrogen bond position. Since the enol and imine entangled protons on ***G′*** are one-half of the four-entangled imine and enol ***G′-C′*** proton qubit-pairs, enzyme quantum reader measurements on ***G′***-proton states specifically select quantum mechanical qubit states, $|-\rangle$ and $|+\rangle$, for the four entangled ***G′-C′*** protons. Here the entangled pair — guanine carbon-2 imine and cytosine carbon-2 enol — are identified, respectively, as proton numbers I and II (Roman numerals). Proton numbers III and IV, respectively, are cytosine carbon-6 imine and guanine carbon-6 enol. Using this notation, the enzyme quantum reader measures the four entangled proton qubit states of ***G′0 0 2*** as $|-+-+\rangle$, i.e., guanine imine proton I is in state $|-\rangle$, cytosine enol proton II is in state $|+\rangle$, cytosine imine proton III is in state $|-\rangle$, and guanine enol proton IV is in state $|+\rangle$. Similarly, the proton qubit state for ***G′2 0 2*** is $|-++-\rangle$, and is $|+-+-\rangle$ for ***G′2 0 0***, and finally, is $|+--+\rangle$ for eigenstate ***G′0 0 0***. In addition to the four quantum mechanical states of ***G′*** imposed by enzyme quantum reader measurements (Figure 3b-e), twelve additional states are required to specify the four, two-state quantum mechanical proton qubits. The ***G′-C′*** site superposition consists of two sets of intramolecular entangled proton qubit-pairs that are participating in quantum oscillations, $|+\rangle \rightleftarrows |-\rangle$, at ~$10^{13}$ s–1 between near symmetric energy wells in decoherence-free subspaces [16-19,23-25,45]. Therefore, the most general quantum mechanical state of these four ***G′-C′*** protons is given by

$$
\begin{aligned}
|\Psi\rangle = \; & c_1|-+-+\rangle + c_2|---+\rangle + c_3|--++\rangle + c_4|-+++\rangle \\
& + c_5|-++-\rangle + c_6|----\rangle + c_7|-+--\rangle + c_8|--+-\rangle \\
& + c_9|+-+-\rangle + c_{10}|+++-\rangle + c_{11}|++--\rangle + c_{12}|+---\rangle \\
& + c_{13}|+--+\rangle + c_{14}|++++\rangle + c_{15}|+-++\rangle + c_{16}|++-+\rangle,
\end{aligned}
\tag{6}
$$

Where the *ci*'s represent, generally complex, expansion coefficients. Since the 16-state superposition of four entangled proton qubits occupy enol and imine "intra-atomic" subspaces, shared between two indistinguishable sets of electron lone pairs, the entangled quantum superposition system will persist in evolutionarily selected decoherence-free subspaces until an invasive perturbation, e.g., "measurement", exposes the previously "undisturbed" quantum mechanical superposition [16-19,23-25,,45-46]. Just before enzyme quantum reader measurement of a ***G′-C′*** site, where ***G′*** is on the transcribed strand, the 16-state ***G´-C´*** superposition system is described by Eq (6). In intervals, $\delta t << 10^{-13}$ s, the enzyme quantum reader "simultaneously" detects entangled ***G′***-protons I (carbon-2 imine) and IV (carbon-6 enol) in either correlated position states, $|->$ or $|+>$, which are components of an entangled proton "qubit-pair". When proton I or IV is measured by the quantum reader in position state, $|->$ or $|+>$, the other member of this entangled pair will, *instantaneously,* be in the appropriately correlated state, $|+>$ or $|->$, respectively. Protons detected in state $|->$, "outside" groove position, form "new" entanglement states with the proximal quantum reader [1,16-20], which enable enzyme quantum coherence to implement its quantum search, $\Delta t' \leq 10^{-14}$ s. This specifies an incoming electron lone-pair, or amino proton, belonging to the tautomer selected for creating the "correct" complementary mispair (Figure 6). Protons detected in state $|+>$, "inside" hydrogen bonding position, contribute to specificity of the ***G′*** genetic code, exemplified by both ***G′2 0 2*** and ****C2 0 2²*** "measured as" normal $T2^2$ 0 2^2 (Figure 5) via "quantum measurements" that yield observable transcription and replication [16-19,35-36,42-44]. Since the quantum reader detects entangled ***G′***-protons I and IV in states $|->$ or $|+>$, the "matching" correlated quantum states, $|+>$ or $|->$, of entangled ***C′***-protons II and III were *instantaneously* specified. Consequently, enzyme quantum reader "measurement" on ***G′***-protons I and IV converts, instantaneously, the 16-state quantum system of Eq (6) into the 4-state system — $ć1|-+-+\rangle$, $ć5|-++-\rangle$, $ć9|+-+-\rangle$, $ć13|+--+\rangle$ — listed in column **B** of (Table 1) and illustrated in (Figure 3b-e), where expansion coefficients, *ći,* are defined by *ć1* = Σ4i = 1 *ci*, *ć5* = Σ8i = 5 *ci*, *ć9* = Σ12i = 9 *ci*, and *ć13* = Σ16i = 13 *ci*. This result is displayed in (Table 1) where column **A** identifies the unperturbed 16-state quantum system of Eq (6). Column **B** contains the distribution of $|->$ and $|+>$ proton states — for ***G′-C′*** protons: I, II, III, IV — generated instantaneously because of the quantum reader initially "measuring" quantum states of entangled ***G′***-protons I and IV. The instantaneously generated quantum states — $ć1|-+-+\rangle$, $ć5|-++-\rangle$, $ć9|+-+-\rangle$, $ć13|+--+\rangle$ — provide, instantaneously, specific instructions for the enzyme – proton entanglement *before* it embarks on its entangled enzyme "quantum quest", $\Delta t' \leq 10^{-14}$ s, of selecting the incoming tautomer specified by molecular evolution, ***ts*** requirements [17-18,35-36,42-44]. Incoming tautomers selected by entangled enzyme quantum searches are identified in column **C** and resultant molecular clock substitutions, ***ts,*** are listed in column **D** of Table 1.

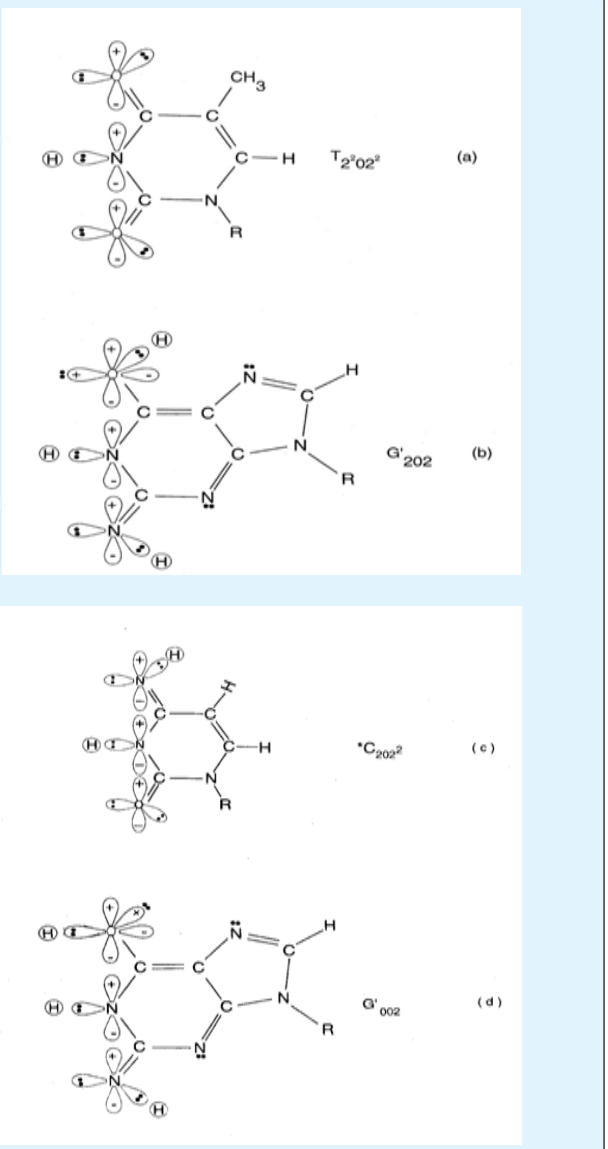

Figure 5: Approximate proton–electron hydrogen bonding structure "seen by" Grover's [20] enzyme quantum reader in intervals, $\delta t << 10^{-13}$ s, encountering (a) normal thymine, $T2^2\ 0\ 2^2$; (b) enzyme-entangled enol-imine ***G'2 0 2***; (c) enzyme-entangled imino cytosine, ****C2 0 2²***, and (d) enzyme-entangled enol-imine ***G'0 0 2***. Notation is specified in Figure 3 legend.

In intervals, $\delta t << 10^{-13}$ s, the enzyme quantum processor measurement apparatus "traps" entangled ***G'*** imine and/or enol protons — I and IV — in DNA grooves, specified by state $|$–>, and consequently, the position state, $|$–> or $|$+>, is instantaneously specified for the four entangled ***G'-C'*** protons: I, IV and II, III. In column **A** of Table 1 an entanglement state between the quantum reader and a "groove" proton is indicated by superscript, "*", e.g., |*–+–+>, identifies ***G´*** proton I as the enzyme – entangled "groove" proton. The "new" entanglement state between the quantum reader and the "trapped" proton enables enzyme quantum coherence to be immediately exploited in implementing an entangled enzyme quantum-search, $\Delta t' \leq 10^{-14}$ s, which ultimately specifies the ***ts*** as ***G'0 0 2*** → *C*, ***G'2 0 2*** → *T* or ***G'2 0 0*** → *G* (Table 1). The specificity of each ***ts*** is governed by the entangled enzyme quantum search selecting the *correct* incoming tautomers — *syn*-$G2^2$ 2 #, *syn*-$A0^0$ 2 #, $C0^0$ 2 2^2 — respectively, for proton qubit eigenstates — ***G'0 0 2, G'2 0 2, G'2 0 0*** — illustrated in Figure 3, Tables 1 & 2 [17-18,35-36]. Natural selection has exploited entanglement properties of EPR-generated entangled proton qubits which allow enzyme – proton entanglement to specify, and implement, results of an entangled enzyme quantum search in intervals, $\Delta t' \leq 10^{-14}$ s [10-12,16-20]. This mechanism implies that enzyme – proton entanglement implementation of an enzyme quantum search would *not* be successful without instantaneous specification of the four ***G' C'*** entangled proton qubit states determined by quantum reader "measurements" on the two ***G'***-proton qubits, I and IV, associated with the transcribed strand [10-12] (Table 1).

A	B	C	D
c_1 | *–+–+> c_2 | *–––+> c_3 | *––++> c_4 | *–+++>	c_1 | –+–+> c_2 | –+–+> c_3 | –+–+> c_4 | –+–+>	syn-$G2^2$ 2 #	***G'0 0 2*** → C
c_5 | *–++*–> c_6 | *–––*–> c_7 | *–+–*–> c_8 | *––+*–>	c_5 | –++–> c_6 | –++–> c_7 | –++–> c_8 | –++–>	syn-$A0^0$ 2 #	***G'2 0 2*** → T
c_9 | +–+*–> c_{10} | +++*–> c_{11} | ++–*–> c_{12} | +––*–>	c_9 | +–+–> c_{10} | +–+–> c_{11} | +–+–> c_{12} | +–+–>	$C0^0$ 2 2^2	***G'2 0 0*** → G
c_{13} | +––+> c_{14} | ++++> c_{15} | +–++> c_{16} | ++–+>	c_{13} | +––+> c_{14} | +––+> c_{15} | +––+> c_{16} | +––+>	none	***G'0 0 0*** → ? ? = microcosmony

Unperturbed (A) and instantaneous yield of "measured" (B) G′-C′ entangled proton qubit states, showing results of entangled enzyme quantum search, $\Delta t' \leq 10^{-14}$ s, (C) and molecular clock (D) results, ts.

Table 1: Evolution of the sixteen-state entangled proton qubit G´-C´ superposition, before measurement (column A), after measurement, $\Delta t' \leq 10^{-14}$ s (column B), and decohered observables (column D).

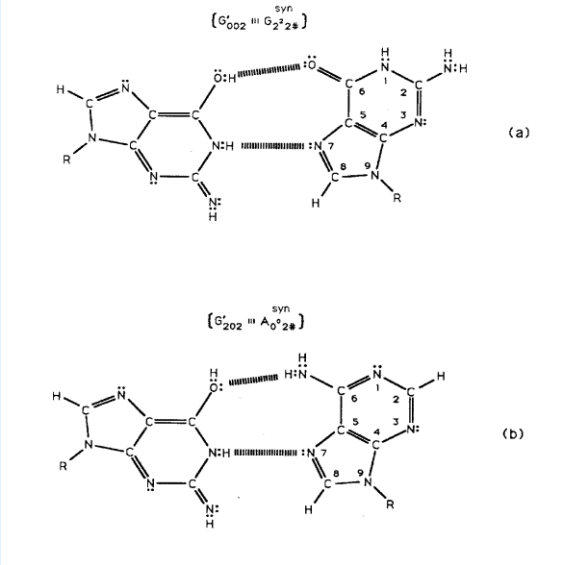

Figure 6: Complementary transversion mispairs created by enzyme-proton entanglement executing a "truncated" Grover's quantum search. Complementary mispairs between (a) enol-imine ***G′002*** (Figure 5b) and *syn*-guanine (*syn*-G2^{2}2#) and (b) enol-imine ***G′202*** (Figure 5c) and *syn*-adenine (*syn*-A0^{0}2#). The # symbol indicates the position is occupied by ordinary hydrogen unsuitable for hydrogen bonding.

Grover's Enzyme – Proton Entanglement Quantum Search

Grover's-type enzyme quantum reader patrols the double helix along major (~ 22 Å) and minor (~ 12 Å) grooves, creating entanglement states between "measured" enol and imine entangled qubit "groove protons" and proximal enzyme components [16-19,20,38]. The quantum reader polymerase energy source is ATP and it maintains a reservoir of purines, pyrimidines and nucleotides for base pairing operations. Davies has noted that the polymerase protein has a mass of about 10^{-19} g, and a length of about 10^{-3} cm and travels at a speed of about 100 bp per sec., or about 10−5 cm s^{-1} [48-49]. Curiously, the normal speed of the polymerase, ~ 10^{-5} cm s^{-1}, corresponds to the limiting speed allowed by the energy-time uncertainty relation for the operation of a quantum clock. For a clock of mass m and size l, Wigner found the relation

$$T < ml^2/\hbar \quad (7)$$

Equation (7) can be expressed in terms of a velocity inequality given by

$$\mathbf{v} > \hbar/m\,l \quad (8)$$

which, for this polymerase, yields a minimum velocity of about 10^{-5} cm s^{-1}, implying the quantum reader enzyme speed of operation can be confined by a form of quantum synchronization uncertainty [48,50]. The quantum reader "measurement apparatus" has been evolutionarily selected to decipher, process and exploit informational content within DNA base pairs composed of either (*a*) the classical keto-amino state, (*b*) undisturbed, enol and imine entangled proton qubit states — Eqs (2 – 6) — including enzyme – proton entanglements participating in an entangled enzyme quantum search, $\Delta t' \leq 10^{-14}$ s [16-20,31,42-45].

The enzyme quantum measurement-operator is identified by *M,* and operates on ***G′***-proton states located on the transcribed strand to yield three different entanglement states between groove protons and enzyme components. From column **B** of Table 1 these enzymatic quantum "measurements", and resulting enzyme-proton entanglements, can be represented by

$$M\,|\,-+-+>=\acute{c}1\,|\,-+-+>\hat{E}p_{\mathrm{I}} \quad (9)$$
$$M\,|\,-++->=\acute{c}5\,|\,-++->\hat{E}p_{\mathrm{I}}, p_{\mathrm{IV}} \quad (10)$$
$$M\,|\,+-+->=\acute{c}9\,|\,+-+->\hat{E}p_{IV}, \quad (11)$$

where $\hat{E}p$I, pIV in Eq (10) represents quantum entanglement between "groove" proton I (***G′2 0 2***-imine) and "groove" proton IV (***G′2 0 2***-enol) and proximal enzyme components. Similarly, $\hat{E}p$I and $\hat{E}pIV$, represent alternative entanglements between enzyme components and entangled proton I, and separately, entangled proton IV, respectively. The original unperturbed groove proton's "quantumness" becomes distributed over an enzyme "entanglement site", which is selected to complete its assignment of specifying the complementary mispair before proton decoherence, i.e., $\Delta t' < \tau_D < 10^{-13}$ s [16-19,31]. Each of the three enzyme-proton entanglements implements a different "selective" quantum search, $\Delta t' \leq 10^{-14}$ s to specify the *correct* evolutionarily required purine or pyrimidine tautomer to properly complete the molecular clock base substitution, ***ts,*** by a quantum processing Topal-Fresco substitution-replication mechanism (Tables 1 & 2; Figure 6) [16-20,35,36,42-45,51-57]. Since quantum informational content is deciphered by enzymatic processing of entangled proton qubits shared between two indistinguishable sets of electron lone-pairs, the entangled enzyme quantum search mechanism is assumed to initially select the incoming tautomer, based on electron lone-pair, or amino proton, availability. Evidently the "evolved" quantum

reader has an immediately accessible "reservoir" of required tautomers for quantum search selection [17-19,47].

Evidence discussed here implies EPR-generated entangled proton qubits are "measured", $\delta t << 10^{-13}$ s, by Grover's [20] quantum reader-processor, which specifies an entangled enzyme quantum search, where quantum information processing, $\Delta t' \leq 10-14$ s, is executed [1-2,10-12,16-20,23-25,42-45,54-56]. The evolutionarily available purine and pyrimidine database is "searched" for the "matching" classical tautomer *required* to execute an "in progress" complementary mispair formation before proton decoherence, $\tau_D < 10^{-13}$ s [16-19,31]. The initial component of the complementary mispair — the selected eigenstate — was specified by "new" quantum entanglement between the "trapped" entangled groove proton and the enzyme quantum reader (Table 1). The enzyme – proton entanglement implements a quantum search which specifies — in intervals, $\Delta t' \leq 10^{-14}$ s — the incoming electron lone-pair, or amino proton, belonging to the tautomer required to create the complementary mispair (Figure 6; Table 1) [16-20,31]. This allows quantum coherence of the entangled ribozyme and/or enzyme to specify the ***ts*** or ***td***, and thus, enable entanglement-directed genomic evolution [1,16-20,44-45,51]. Grover's-type [20] measurements of entangled proton qubit states occupying ***G´-C´, *G-*C*** and ****A-*T*** sites specify instructions for quantum information processing execution, which generate time-dependent substitutions, ***ts*** exhibited as — ***G′2 0 2 → T, G′0 0 2 → C, *G0 2 0⁰ → A & *C2 0 2² →T*** (Tables 1 & 2; Figure 3) but time-dependent deletions, ***td***, are manifested as ****A*** → deletion and ****T*** → deletion (Figure 4) [17-18,35-36]. Measurements identify the relation, rates ***ts*** ≥ 1.5-fold rates ***td***; so, ***ts*** + ***td*** generates random genetic drift which explains the slight A-T richness exhibited by human genomic systems [19,35-36,47,51-53,58]. The EPR-entanglement algorithm yields molecular clock ***ts*** and ***td,*** *after* (***i***) an initial formation of enzyme-proton entanglement, $\delta t << 10-13$ s, (***ii***) quantum information processing via an enzyme entanglement-assisted quantum search ($\Delta t' \leq 10-14$ s), (***iii***) selection of the next amino acid for protein growth, (***iv***) specification of the "correct" complementary mispair (Figure 6) and (***v***) selected replication-substitution or deletion with classical tautomers containing decohered protons [1,2,16-19,35,36,44]. Consistent with implementing steps — (***i***), (***ii***), (***iii***), (***iv***), (***v***) — ***ts*** and ***td*** can introduce and eliminate initiation codons — UUG, CUG, AUG, GUG — and termination codons, UGA, UAA, UAG [1-2,16-18]. The resulting "dynamic mutations" can cause susceptible microsatellites [2,17-18,59-62], e.g., (CAG)n (n > 36), to exhibit deletions and/or expansions ≥ 10 (CAG) repeats in 20 y [2,16,59,61-62]. This observable expansion/contraction mechanism [1-2,16-18,59-60] can account for genomic growth, over the past ~3.5 billion y, from primordial RNA [63-66] to 21st century DNA of ~ 6.8 ×109 base pairs [1-2,47,51].

Quantum flip flop States	Allowable Pair Formation at Replication						Transcription Message
	Normal Bases				Syn-Purines		
	$G_{2^2 0 0^o}$	$C_{0^o 2 2^2}$	$A_{0^o 2 \#}$	$T_{2^2 0 2^2}$	$G_{2^2 2 \#}$	$A_{0^o 2 \#}$	
G'_{002}					G-C → C-G		U∓
G'_{202}						G-C → T-A	$T_{2^2 0 2^2}$
G'_{200}		Not detectable					$G_{2^2 0 0^o}$
G'_{000}							U
$*G_{020^o}$				G-C → A-T			U
$*G_{220^o}$							U
C'_{220}							U
C'_{020}							U
C'_{022}	Not detectable						$C_{0^o 2 2^2}$
C'_{222}							U
C'_{202^2}			G-C → A-T				$T_{2^2 0 2^2}$
C'_{002^2}							U
$*A_{20\#}$		A-T → G-C				A-T → T-A	U
$*A_{00\#}$					A-T → C-G		U
$*T_{022^2}$	A-T → G-C						$C_{0^o 2 2^2}$
$*T_{222^2}$							U

∓ Undefined

Table 2: Transcribed messages from entangled proton qubit states, decohered isomers and formation of complementary mispairs.

Normal tautomers (top row) and entangled qubit "flip-flop" states/decohered tautomers (left column) are listed in terms of the compact notation for hydrogen-bonding configurations identified in Figure 3. Base pair substitution notation at the respective row-column juncture identifies eigenstate components that will form a complementary mispair with an incoming classical tautomer, selected by an enzyme-entanglement quantum search, $\Delta t' \leq 10^{-14}$ s. Transcribed messages obtained from

measurements of entangled proton qubit states are identified in the right-hand column

Consistent with observation and analyses neither water, ionic incursions or random temperature fluctuations obstruct quantum information processing, $\Delta t' \leq 10\text{–}14$ s $< \tau_D$ executed by evolving rat and human genomes [16-19,21,31,42-45,67]. Since EPR entanglement-enabled quantum information processes are available to evolving rat and human microsatellite distributions evolution arguments imply that analogous quantum information processing algorithms are operationally available to *Homo sapiens'* brain-cell DNA [7,9,16-19,21,68-70]. In this case, analogous quantum information processing algorithms are routinely operational in DNA of human brain-cells which are embedded within an evolutionarily selected neural circuitry [7,16-19,68-70]. Consequently, quantum information processing, $\Delta t' \leq 10^{-14}$ s executed by a single brain-cell could communicate the resulting quantum-informational calculations to the brain's neuronal network of ~ billons of neurons[16-20,31]. Otherwise, EPR-generated entangled proton qubits are available for quantum information processing exhibited by evolving rat and human DNA, but – for some evolutionary reason – availability of EPR-generated, entangled proton qubits is *not* utilized for cognitive processes to implement quantum information processing, which *would* enable existence of human consciousness [7-9,10-12,16-19,44,54-56]. Therefore, this report argues that human consciousness *is* a consequence of an evolutionarily coordinated network of entanglement-enabled, quantum information processing executed by human brain-cells, whose orchestrated quantum information processing allows manifestation of human consciousness[7-9,10,16-19,68-70].

Entanglement-Enabled Model for Genetic Code Origin

The observable, EPR-entanglement algorithm provides a quantum mechanical model for entanglement-enabled origin of the genetic code [17-19,44,47,51]. Based on the quantum information processing model, entangled proton qubit resources were initially introduced into ancestral duplex "loops" of ribozyme – RNA systems [1,16,19,54-56,63-66]. Primordial RNA – ribozyme duplex nucleic acid components are assumed to have been composed of analogs of G – 5HMC (5hydroxymethylcytosine) and A– U [1,5,35-37,47]. Survival of ribozyme – RNA duplex "loops", populated with entangled proton qubits, required their selection by rudimentary quantum bio-processors [20], operating on entangled proton qubits, thereby introducing peptide – ribozyme – proton RNA entanglements. Since quantum bio-processors "measure" quantum informational content by selecting entangled proton qubit states, in intervals $\delta t << 10^{-13}$ s, quantum reader operations can be approximated by a "truncated" Grover's [20] quantum search of "susceptible" unsorted qubit-pair states occupying ***G′-5HMC′*** and ****G-5HM*C*** superposition sites[36,44].

Grover's algorithm is applicable for large system sizes N in high dimensional Hilbert spaces where the quantum enabled database is unsorted. However, a quantum bio-processor searching an unsorted database of N qubit states (here N = 20 qubit states occupying ***G′-C′*** + ****G-*C*** sites; Eqs (2-6)) can be approximated by iterations of a "truncated" Grover's quantum search. The quantum bio-processor is designed to identify entangled proton qubit states, including those occupying a RNA groove, where the "measurement" interval satisfies, $\delta t << 10^{-13}$ s. The quantum bio-processor peptide-ribozyme forms an entanglement state with the "trapped" proton that, before proton decoherence, $\tau_D < 10^{-13}$ s, (*a*) generates quantum transcription information from "measured" entangled proton qubit states, e.g., ***G′2 0 2*** → *U*, ***C′2 0 2²*** → *U*, etc, (*b*) implements a "new" peptide bond between an "incoming" selected amino acid and an existing "in place" amino acid, and (*c*) implements selection of an "incoming" tautomer to "pair with" the ultimately decohered eigenstate, specified by the "trapped" proton (Table 1) in a genome groove [16-19,38,]. In this context, quantum bio-processor operations can be qualitatively approximated by a "truncated" Grover's [20] algorithm. This approximation of a quantum bio-processor measurement on entangled proton qubit states occupying ***G′-C′*** and ****G-*C*** superpositions implies a "truncated" (N = 20 qubit states) Grover's algorithm would yield an improved efficiency of $\sqrt{N}$ over a classical search. If J is the total number of bio-molecular quantum reader measuring operations, Grover's "truncated" algorithm states

$$(2J + 1) \arcsin (1/\sqrt{N}) = \pi/2 \quad (12)$$

which yields the interesting solutions,

$$J = 1, N = 4 \quad (13)$$
$$J = 2, N = 10.4 \quad (14)$$
$$J = 3, N = 20.2 \quad (15)$$
$$J = 4, N = 33.2. \quad (16)$$

Consistent with observables exhibited by T4 phage DNA, the model outlined here assumes quantum reader measurements of ***G′-5HMC′*** and ****G-5HM*C*** superpositions generated RNA "transcription qubits" (Table 2) — ***G′2 0 2*** → *U*, ***G′2 0 0*** → *G*, ****C2 0 2²*** → *U*, ****G0 2 0⁰*** → ***A*** — that

provided single base RNA informational units as precursor mRNA and precursor tRNA. Measurements imply that ***C2 0 2²** → *T* yields ***G0 2 0⁰** → *A* (~ 100%) in the complementary strand. Precursor tRNA components were evidently retained in the bio-molecular quantum processor's "hard drive" reservoir until a sufficient "sampling" of entangled qubit states had been subjected to the set of measurements [36,44]. In this case, the number of measurement operations, J, converged to a value that yielded adequate statistics. According to this qualitative model, the quantum entanglement algorithm, implemented by ribozyme – peptide quantum reader-processors, converged via natural selection, to three measurement operations — J = 3 in Eq (15) — to obtain adequate statistical probabilistic measurements of 20 entangled proton qubit states occupying ***G′-5HMC′*** and ***G-5HM*C*** superposition sites; ***A-*U*** sites were deleted [17-18,35-36]. The three selected quantum processor measurements identified a triplet code for a precursor tRNA, where L-amino acids were selected. Three separate probabilistic measurement operations would "quantify" a sufficient number of the 20-different entangled proton qubit states, and, specify about 20, i.e., 22, amino acids for participation in protein structure [5,47].

The scenario outlined here implies quantum reader measurements of entangled proton qubits occupying ancestral ***G′-5HMC′***, ***G-5HM*C*** and ***A-*U*** superposition sites may have provided the initial quantum informational content, specifying evolutionary parameters for origin of the genetic code, consisting of ~ 22 L-amino acids specified by 4^3 triplet codons. Descriptions of EPR-generated entangled proton qubits require appropriate quantum entanglement models which further imply a plausible explanation for origin of the genetic code [1-2,5,16-17,19,47]. Such "fundamental" quantum entanglement evolutionary developments in primordial ribozyme – RNA systems have been evolutionarily retained in operational eukaryotic systems [1, 5, 16-19,47,63-66].

Consequences of EPR-Proton Qubit Correction to Muller's Constant "Mutational Load"

Most 21st-century discussions of biological noise, N(t) are in terms of Muller's classical, constant "mutational load", dN/dt = λ, which neglects time-dependent EPR-entanglement contributions [5,16-19,44,45,47,52-53,58-59,71-76]. Since quantum entanglement terms *cannot* be efficiently simulated by classical mechanisms, the time derivative of *total* biological noise is more accurately expressed in terms of an exclusively classical component, λ [71], *plus* quantum entanglement contributions, βt [13-19,54-56]. A 3-level quantum approximation for the probability, P_ρ (t), of EPR-arrangement, *keto-amino —(entanglement) → enol-imine* is given by P_ρ (t) = ½ $(\gamma_\rho / \hbar)^2$ t^2 (see Appendix), where γρ is the energy shift between the initial metastable and final product entanglement state, and ρ = 1, 2 for symmetric, asymmetric channels (Figures 2&3), and ħ is Planck's constant divided by 2π [16,19,39,42-45]. Thus $dP/dt = (\gamma_\rho /\hbar)^2 t = \beta t$, where $\beta = (\gamma_\rho /\hbar)^2 \approx 2x10^{-23}$ s^{-2} (W G Cooper, unpublished results); so, the time derivative of the *total* biological noise, dN/dt, accumulating in the gene, g, is more accurately expressed by the sum of classical plus EPR-entanglement contributions given as

$$dN/dt = \lambda + \beta t \quad (17)$$

Quantum entanglement contributions are approximated by the βt term in Eq (17), which is *purely* quantum mechanical, and is obtained from the 3-level quantum approximation to EPR arrangements, *keto-amino → enol-imine* (Appendix) [13-19,47,71]. Classical considerations of biological information processing treat molecular informational dynamics in terms of arrangements and rearrangements of classical "ball-and-rod" molecular units that store and process classical information digital bits [10-12,48,55]. But quantum informational content embodied within entangled proton qubit super positions (Figures 2-4; Table 1) — ***G′-C′, *G-*C, *A-*T*** — occupying intramolecular decoherence-free subspaces *requires* enzyme – proton entanglement measurement and processing, where a proton qubit eigen state is quantum mechanically selected, by Grover's processor [20], to specify observable ***ts*** or ***td*** [1-2,10-20,23-25,35-36,42-44].

Robust *Homo sapiens* inherit normal, evolutionarily conserved "cancer genes" "Alzheimer's genes" and the *huntingtin gene* each of which is associated with its "wild-type" conserved noncoding genomic space, CNGS, *s* defined, approximately, by the inequality, $1 \geq s \geq 0.97$ [16-19,42-44,61,62,76-88]. This discussion considers three different sets of Q individuals (Q ≥ 100,000) – the populations – who have inherited normal target domains, *s* ($1 \geq s \geq 0.97$), which includes conserved "cancer genes", "Alzheimer's genes" and the *huntingtin gene*. After developing the EPR-entanglement Darwinian polynomial, each of the three age-related genetic diseases can be evaluated for genotypic and phenotypic expression, as a function of classical and quantum entanglement genetic contributions [16,18-19]. Age-related cancer systems are evaluated here [77]. A general expression for the total

biological noise, N(t), in all Q individual genes, g, in the population at age t is given by

$$N(t) = Q\{N_0 + \sum_{i=1}^{m} \lambda_i t + \sum_{j=1}^{k} (\beta_j/2)\, t^2\}, \qquad (18)$$

Where N_0 is the average number of mutations – originating by classical and entanglement channels – per gene g in the population of Q at t = 0. The sum $\Sigma^{m}{}_{i} = 1$ is over all m G-C + A-T pairs in the relevant gene where mutations originate by classical Newtonian operations on DNA [47,71,89]. The sum $\Sigma^{k}{}_{j}=1$ is over the k G-C + A-T pairs in the gene (generally, m = k) where quantum uncertainty limits, $\Delta x\, \Delta p_x \geq \hbar/2$ are imposed on metastable hydrogen bonding amino protons, creating confined spaces, Δx, which cause direct quantum mechanical proton – proton physical interaction [32-33]. This generates probabilities of EPR-arrangements, *keto-amino → enol-imine,* such that position and momentum entanglement is introduced between separating enol and imine protons [10-20,35-36]. Product enol and imine proton qubits are shared between two indistinguishable sets of electron lone-pairs, belonging to enol oxygen and imine nitrogen in decoherence-free subspaces on opposite strands, and consequently, participate in entangled quantum oscillations, at ~ $4x10^{13}$ s^{-1}, between near symmetric energy wells until "measured by", δt << 10^{-13} s, Grover's quantum reader [16-20,23-25,45]. The EPR-entanglement algorithm yields molecular clock ***ts*** and ***td,*** *after* (***i***) an initial formation of enzyme-proton entanglement, δt << 10^{-13} s, (***ii***) implementation of an entanglement-assisted enzyme quantum search ($\Delta t' \leq 10^{-14}$ s), (***iii***) selection of the next amino acid for protein growth, (***iv***) specification of the "correct" complementary mispair (Figure 6), and (***v***) selected replication-substitution or deletion with classical tautomers containing decohered protons. The βt_2 term in Eq (18) is obtained from a 3-level quantum approximation to EPR arrangements *keto-amino → enol-imine* (see Appendix) [1-2,16-19,42-45]. However, $\Sigma_j\, \beta_j t^2$ terms are experimentally contributing observables *if and only if* quantum entanglement processes — (***i***) through (***v***) above — are properly executed by the enzyme quantum processor [16-20].

Consistent with observation, this model assumes that target gene g can — because of accumulating an evolutionarily defined level of EPR-generated entangled proton qubits (*stochastic* mutations) plus classical "point" mutations — be "converted" into a disease producing mode [16-19, 35-37,42-44,47,51-53,*71,89*]. The time rate of change of converted target genes, dg(t)/dt, is proportional to the total number of entangled proton qubits in the relevant genetic domain plus classical, replication-dependent Newtonian mutations contained in each of the Q genes, g(t), in the population at age t. This is given by

$$d/dt\, g(t) = 1/K\, N(t) \quad (19)$$

where 1/K is the proportionality constant, and N(t) is the noise defined in Eq (18). The number of converted target genes, g (t), in the population of Q at age t is given by

$$g(t) = g_0 + Q/K\, \{N_o\, t + \sum_{i=1}^{m} (\lambda_i/2)\, t^2 + \sum_{j=1}^{k} (\beta_j/6)\, t^3\}, \qquad (20)$$

where g_0 is the number of converted genes in the population at t = 0. Phenotypic expression incidence, E(t), in the population of age t would change at a rate, dE/dt, which is proportional to the total number of converted genes, g(t), in the population. This relationship is expressed as

$$d/dt\, E(t) = 1/B\, g(t) \quad (21)$$

where 1/B is the proportionality constant. The incidence of phenotypic expression, E(t), in the population at age t is given as

$$E(t) = E_0 + (g_o/B)\, t + Q/2KB\, \{N_0\, t^2 + \sum_{i=1}^{m} (\lambda_i/3)\, t^3 + \sum_{j=1}^{k} (\beta_j/12)\, t^4\},$$

where E_0 is the incidence at t = 0. Here time t = 0 when the egg is fertilized. If the *s*-domain in the "*cancer gene*" or "*Alzheimer's gene*" were populated by entangled proton qubits to its threshold limit at conception, i.e., to $s \approx 0.97 + \varepsilon$, the model implies spontaneous abortion would be a consequence so, a live birth implies $E_0 = g_0 = 0$ at t = 0 in Eq (22) [2,19,90]. Therefore, N_0 is the average number of inherited mutations per gene, including classical and entanglement-originated ***ts*** + ***td*** accumulated in CNGS in prior generations. Entangled proton qubit states *per se* are not inherited but accumulate with time at rates governed by quantum uncertainty limits, $\Delta x\, \Delta p_x \geq \hbar/2$, operating on metastable hydrogen bonding amino DNA protons [16-19,34-36,44,61,91].

Equation (22) can evaluate entanglement-originated and classical contributions to genotypic and phenotypic expression of disease [16-19]. The 74 "class 1" tumors identified by the Connecticut Tumor Registry between 1968 and 1972 generate the empirical cancer incidence as a function of age (ages 10 to 80 y) data displayed in Figure 7 [77]. Average percentage total incidence as a function of

age is proportional to t^4, and differences between male and female incidence curves in Figure 7 are negligible [77]. "Class 1" tumors are identified as those that exhibit a single incidence peak at age > 50 y, whereas "class 2" tumors (e.g., bone, lymphatic leukemia, testis and Hodgkin's disease; data not shown) exhibit two incidence peaks; one at age < 35 y and one at age > 50 [77]. Consistent with observation and age-related cancer incidence shown in Figure 7, Eq (22) distinguishes between EPR-generated entanglement-enabled contributions – "driver mutations", specified by $\Sigma_j\beta_j\ t^4$ – and classically introduced "passenger mutations", designated by $\Sigma i\ \lambda i\ t^3$. Both age-related cancer incidence Figure 7 and quantum entanglement contributions to disease, $\Sigma_j\beta_j\ t^4$ in Eq (22), are described by "smooth" ~ t4 curves, implying classical, $\Sigma i\ \lambda i\ t^3$ – "passenger mutation" terms – do *not* contribute to ~ t^4 cancer incidence data in Figure 7, which is consistent with observation [76-80]. In this case, age-related cancer [77], exhibited in Figure 7, is a consequence of normal, evolutionarily selected quantum entanglement algorithm processes $\Sigma_j\beta_j\ t^4$, introducing cancer-causing "driver mutations" which originate from measurements on EPR-generated entangled proton qubits [1,16-19,76,78-80]. This assessment concludes that age-related cancer incidence data, Figure 7 are described by EPR-generated quantum entanglement contributions, $\Sigma_j\beta_j\ t^4$ in Eq (22); so, classical mechanisms – "passenger mutations", $\Sigma i\ \lambda i\ t^3$ – do *not* contribute to age-related cancer incidence exhibited in Figure 7 [19].

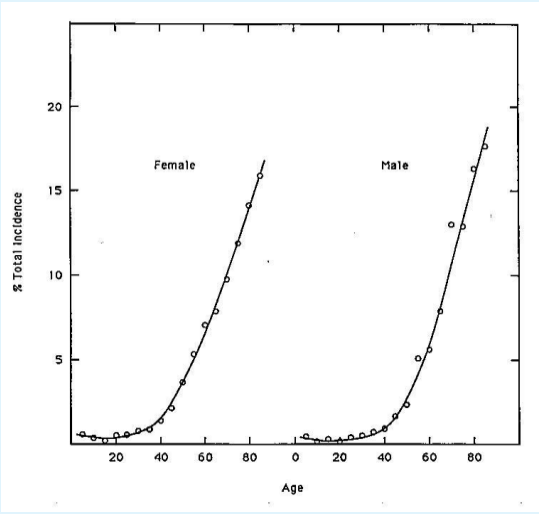

Figure 7: Cancer incidence as a function of age [77]. Average age distribution of all "Class 1" tumors (those with single incidence peak at age > 50 y) classified by the Connecticut Tumor Registry between 1968 and 1972.

Serious efforts to *accurately* understand age-related diseases – exhibited as consequences of entanglement-enabled "point" mutations, ***ts*** + ***td***, acquired by conserved genes– require recognition and understanding of EPR-generated entangled proton qubits, and their biological consequences [16-19,61,77-86]. Since the anti-entanglement hypothesis is falsified, realistic molecular assessments of age-related disease require "proper" inclusion of entanglement-enabled information processing, which has generally been neglected by "classical-only" experimental designs and analyses [16-21,30,54-56,72-76]. Such neglect of EPR-generated entangled proton qubits' contribution to age-related cancer manifestation provides an explanation for the "slow" progress in resolving "cancer questions", when "classical-only" restrictions excluded EPR-generated entangled proton qubits' contributions[18-19, 74-75,77].

Conserved genes that exhibit age-related lethal diseases because of "point" mutations, ***ts*** + ***td*** — e.g., "cancer genes" and "Alzheimer's genes — have been evolutionarily selected to prevent "unsafe" entangled proton qubits' contribution to the "gene pool" [18-19,35-36,42-44,76-86]. When a conserved "cancer gene" acquires entangled proton qubits to its "threshold limit", $s \approx 0.97 + \varepsilon$ unsafe haploid genes are eliminated by spermatogenesis or oogenesis, but corresponding "unsafe" diploid genes manifest cancer [18-19,42-43,78-80]. These conserved genes provide a *necessary* function for species survival, since they disallow evolutionarily depleted genomes — containing "unsafe" levels of entangled proton qubits — from contributions to the "gene pool", thereby "selecting against" evolutionary extinction [77-86]. This conclusion is not obvious without recognizing "stable" EPR-generated entangled proton qubits as origins of entanglement-enabled information processing [16,19,42-43].

Implied Role of EPR-Proton Qubit–Pairs in Operational Dynamics of Brain-Cell DNA Functions

Recent reports present evidence that EPR-generated entangled proton qubits provided resources that enabled primordial RNA – ribozyme systems to embark on quantum information processing algorithms, which selected duplex genomic systems, ultimately yielding double helical DNA [1-5,16-19,35-36,43-47,51,54-56, 63-66]. Consequently, quantum information processing of entangled proton qubits has been integrated into evolutionary dynamics where selection is implemented in terms of entanglement-enabled information processing

[16-19,51-53]. This long history, ~ 3.5 billion y of quantum information processing of EPR-generated entangled proton qubits implies generalized participation for EPR-proton qubits in selecting biologically relevant functions, including *Homo sapiens'* consciousness [1-2,5,6-9,17-19,68-70]. This and previous reports argue that without integration of EPR-generated entangled proton qubits into primordial genomic systems, conscious *Homo sapiens* would be absent[5,35-36,63-66].

Since EPR-generated entangled proton qubit-pairs are exhibited by "expanded" Huntington's disease, $(CAG)_n$ repeats, and by human and rat microsatellite evolutionary distributions, this discussion assumes that EPR-generated entangled proton "qubit-pairs" are resources for quantum information processing in *all* double helical DNA systems, including human brain-cell DNA [1,7,9,17-19, 21,35-37,42-44,51,59, 61,62,68-70,76-86]. In this case, a model for *Homo sapiens'* consciousness is implied by ~ $3.6x10^9$ y of entanglement-enabled evolution, from duplex RNA–ribozyme segments, into double helical DNA of ~ $6.8x10^9$ bp, which resides in *Homo sapiens'* brain-cells [1,5,6-9,16,18,19,47,51].

The evolved human brain contains sensory "biological files" for vision, acoustics, vocal, olfactory, touch, taste, balance, self-motion, pain, emotion, language, analyses, music, imagination, "truth" and "fantasy" [7,18,68-70]. Sensory files are interfaced with, initially vacant, "hard drive" memory files that acquire input data from one or all sensory files. Each "new" experience (stimulus) generates input data for "hard drive" memory files. This stimulus creates an entanglement state between the "measured", entangled groove-proton "qubit-pair" and Grover's enzyme quantum processor, which executes quantum information processing, $\Delta t' \leq 10^{-14}$ s, *before* proton decoherence, $\tau_D < 10^{-13}$ s [1,16,19,31]. The sequence of acquired input events, e.g., successfully riding a bicycle, is "permanently" stored within sequences of G-C rich triplet repeats — e.g., (C*X*G)n, where *X* is G, C, A or T — populated by EPR-generated entangled proton qubits [16].

Brain-cell DNA of robust human infants contains CNGS and conserved genes that have been evolutionarily selected to accumulate "stable" EPR-generated entangled proton qubits, for purposes of executing quantum information processing [16,87-88,92]. Inherited brain-cell DNA systems cannot manifest consequences of quantum informational content until relevant CNGS and genes have been populated with EPR-generated entangled proton qubits to their "threshold limits" [16,91]. This is incrementally achieved by age ~25 y for *H. sapiens.* Brain-cell systems of EPR-generated entangled proton qubits are "measured by" Grover's [20] processors, $\delta t << 10^{-13}$ s, which specifies quantum information processing, $\Delta t' \leq 10^{-14}$ s, but immediate, subsequent replication is not implemented [1,17-18,35-36]. When EPR-generated entangled proton qubit-pairs populate DNA sequences *not* evolutionarily specified for normal quantum information processing in neurological cells, heritable neurological diseases — e.g., Huntington's disease, congenital myotonic dystrophy and amyotrophic lateral sclerosis (ALS) — are exhibited, thereby protecting the gene pool against "avenues" for evolutionary extinction [18-19,35,42-44,59-62,94-95].

The model for consciousness outlined here allows evolutionarily selected, EPR-generated entangled proton qubit-pairs to be "measured by", $\delta t << 10^{-13}$ s, a Grover's-type [20] transcriptase quantum-reader. This generates consciousness-specific quantum information processing instructions, $\Delta t' \leq 10^{-14}$ s, that are executed by enzyme – proton entanglements [10-12,16-19]. The present discussion of human consciousness assumes are correct in their statement, "…the empirical evidence is compatible with the possibility that consciousness arises from nothing more than specific computations [7]." Coordination and orchestration of the numerous, evolutionarily selected, quantum information processing instructions within brain-cell DNA could, in this case be responsible for specifying relevant reactive processes responsible for the phenomenon of human consciousness [6-9,16-19,68-70]. In this consideration, consciousness is exhibited as consequences of execution of "coupled" quantum information processing calculations [7,16-20,54-56]. Unlike the Hameroff-Penrose Orchestrated Objective Reduction (Orch OR) model of human consciousness, the present model does *not* require participation of quantum gravity, but claims that consciousness *requires* existence of EPR-generated entangled proton qubit-pairs — in brain-cell DNA — that are "measured by", $\delta t << 10^{-13}$ s, a Grover's-type [20] transcriptase quantum-reader, which specifies consciousness-relevant quantum information processing instructions that are executed within intervals, $\Delta t' \leq 10^{-14}$ s [9,10-12,16,-19]. This model provides an entanglement-enabled, biophysical explanation of consciousness in terms of evolutionarily selected, quantum information processing instructions which are initiated and executed by micro-physical quantum processing, genomic operations [1-2,7,16-20,42-44, 54-56]. Hameroff and Penrose claim that electrochemical neural networks alone are inadequate to account for human cognition, and thus, propose the necessity of quantum processing of coherent states in microtubules within dendrites. Their model

invokes an on-going development of quantum gravity, and claims that conscious processes are non-computable, i.e., that no computer can duplicate consciousness. These latter two features are *not* required by the present, EPR-generated entangled proton qubit-pairs, quantum information processing model of consciousness [7,9,10-12,16-20].

Without recognition of *in vivo*, anti-entanglement hypothesis falsification, a large classical 37^0 C human brain in thermal equilibrium with its environment of H2O, ions, atoms and molecules would impose decoherence on quantum states, before allowing entangled, coherent-state contributions to mental processes [7,17-19,21,26-33,67-70]. However, a classical-only brain-cell processing model is inconsistent with EPR-generated entangled proton "qubit-pairs", $|+> \rightleftarrows |->$, that are "measured by", $\delta t << 10–13$ s, Grover's [20] processor, which specifies quantum information processing instructions, $\Delta t' \leq 10^{-14}$ s, to accurately yield rat and human evolutionary distributions of microsatellite DNA [1,16-19,21,67,44]. In these cases, "evolutionary origins" of rat and human are separated by ~ $70x10^6$ y, but observed evolutionary distributions of the 22 most abundant microsatellites common to these two species are accurately predicted by an EPR-entanglement algorithm for evolutionary genomic dynamics [16-18,21,22]. Therefore, EPR-generated entangled proton "qubit-pairs", $|+> \rightleftarrows |->$, occupy decoherence-free subspaces for years to decades before a Grover's [*20*] quantum-reader transcriptase measurement of entangled "qubit-pairs" specifies evolution instructions for the 22 most abundant microsatellites common to rat and human [10-12,16-19,21,23-25]. Analyses confirm quantum entanglement model predictions that Grover's-type enzyme-processor measurements of EPR-generated entangled proton "qubit-pairs" can simulate DNA evolution, and further, identify an entangled proton "qubit-pair" as the smallest "measurable" genetic informational unit, specifying selected evolution instructions with "measured" quantum information [16,19]. Thus, rat and human microsatellite evolution is accurately specified by quantum information processing instructions, obtained from Grover's-type [20] "measurement", $\delta t << 10^{-13}$ s, of EPR-generated entangled proton "qubit-pairs", $|+> \rightleftarrows |->$[10-12,16-19,21]. Analogous measurements on EPR-generated entangled proton qubit-pairs in human brain-cell DNA imply availability of an evolutionarily selected, quantum information processing mechanism for executing human consciousness [6-9,16-20,68-70].

Quantum information processing of EPR-generated entangled proton qubit-pairs in brain-cell DNA implies a "mode-of-action" for anesthetic drugs to cause sudden transitions from consciousness to unconsciousness [16-19,54-56,96]. Consistent with quantum information processing of EPR-generated entangled proton qubits in brain-cell DNA, anesthetics inhibit normal activity of Grover's-type enzyme quantum-readers that are responsible for "measuring" quantum informational content of EPR-generated entangled proton qubit-pairs [16-20]. By inhibiting Grover's enzyme quantum-reader of EPR-generated entangled proton qubits, anesthetics impede instructions for implementing quantum information processing [96]. In this case, abrupt transitions from consciousness to unconsciousness is caused by an absence of entanglement-enabled, quantum information processing instructions. When anesthetic concentration becomes sufficiently dilute, Grover's [20] enzyme quantum-readers re-establish "measuring operations" of quantum informational content within EPR-generated entangled proton qubit-pairs; so, normal consciousness is re-established by instructions for active quantum information processing.

This explanation implies "normal", non-drug-induced sleep is a consequence of "inactive" Grover's [20] processors, which – during consciousness – actively measure quantum informational content of EPR-generated entangled proton qubits. In this case, normal sleep could be a "down-time" condition that allows EPR-generated entangled proton qubits to repopulate "recently measured" segments of double helical DNA, while Grover's processors are "inactive".

Consequences of EPR Entanglement-Enabled Information Processing

Origin of Sustainable Life (OoSL) Emerging from EPR-Proton Qubits within RNA – Ribozyme Polymers

Based on "classical-only" arguments for survival considerations, RNA – ribozyme evolution would be a "dead end" [3-5,63-66]. But subsequent genomic evolutionary history implies selection of "enhanced efficiency" for information processing by primordial ribozyme – RNA systems [1,47,66]. This is explained by acquisition of "T4 phage-like" entanglement-enabled information processing where EPR-generated entangled proton qubits emerged in ancestral duplex ribozyme – RNA segments [1,5,10-12,16,19,35-36,44]. Consequently, primordial genomic information acquired entanglement resources which allowed *necessary* entanglement-enabled information processing to be incrementally developed (Figure 8), consistent with predictions of the quantum

entanglement algorithm [1,16-19]. A schematic of implied entanglement-enabled incremental increases in "genomic versatility" is illustrated in Figure 8.

This model implies life's origin emerged, and was sustained, in terms of sequential, entanglement-enabled evolutionary increments [13-16]. A set of increment arrows (→) in Figure 8 identifies the following sequential (or simultaneous) developments over the three phases of primordial evolution**:** monomers → oligomers → ribozymes → duplication of nucleotides → duplex RNA polymer segments → entangled proton qubits → ribozyme – proton entanglements → quantum transcription of entangled qubit-pairs → quantum translation of entangled qubit information → quantum selection of triplet code → construct polypeptides → enzymes from ribozyme – proton entanglements → replication via enzymes → introduction of repair enzymes → genome chemistry selection, RNA replaced by DNA → duplex DNA genomes, etc.

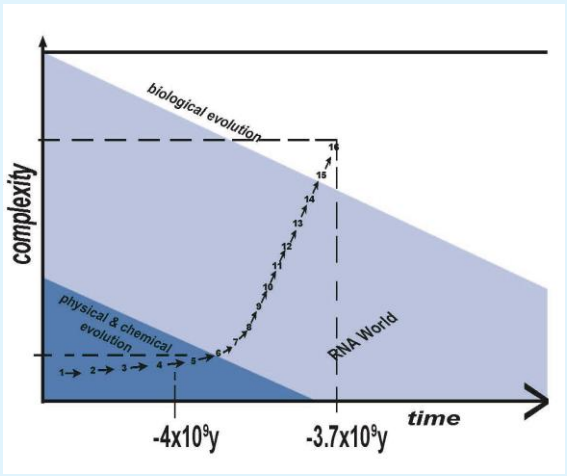

Figure 8: Evolutionary increments during "classical" chemical – physical evolution (dark blue), and during entangled proton qubit-enabled RNA evolution (light blue), yielding duplex DNA systems of regular "biological evolution" (white background). Earliest life-forms are identified at – $4x10^9$ y and earliest stromatolites at – $3.7x10^9$ y [97].

This OoSL (origin of sustainable life) model implies quantum entanglement algorithms, developed and implemented in ancestral RNA – protein systems, were subsequently retained and refined within evolving duplex DNA systems. Classical mechanisms do not explain evolutionary processes between ~ $-4.1x10^9$ y and ~ $-3.7x10^9$ y, but EPR-entanglement algorithm processes provide plausible explanations in terms of quantum information processing [5,13-19,42-44,54-56,97]. This argument allows explanations for origins of quantum information processing algorithms exhibited by ancient T4 phage DNA, rodent – human microsatellite DNA evolution, and 21st-century human genomic systems [16-18,21,35-37,42-44,51,59-61,77,98,]. In this treatment, a reverse-time extrapolation — of proton quantum dynamics required for observable quantum information processing exhibited by ancient T4 phage DNA— appears applicable to analogous, metabolically inert duplex RNA segments occupying primordial pools (0 ^{0}C to 20 ^{0}C, pH 7) of ribozyme – RNA systems [1,5,35-37,63-66, 91,98].

Based on ribozyme – RNA evidence, ancestral RNA genomic structures were susceptible to significant evolutionary pressures that allowed Darwinian selection to exploit "advantageous" applications of quantum information theory [1,5,47,54-56,63-66]. This involved (*a*) the creation and measurement of entangled proton informational qubits, (*b*) quantum/classical genomic informational interfaces, and (*c*) enzyme – proton entanglements that implement quantum searches, $\Delta t' \leq 10^{-14}$ s, to specify synthesis information for a "new" base pair, evolutionary molecular clock event, ***ts*** [1-2,10,16-19, 31,35-36,44]. Also, replacement of ribozyme function with protein enzymes implies peptide-ribozyme – proton entanglement processes selected relevant amino acids to construct the protein enzyme replacement of ribozymes. When ancestral RNA genomes became too massive for acceptable "error-free" duplication, rudimentary repair enzymes were invoked that selected DNA over duplex RNA [1,89,99]. Although enzymatic quantum information processing provided a selective advantage for duplex RNA, as living RNA systems became more complex and versatile, the duplex RNA genome became too "massive" for acceptable error-free duplication [1-2,5,99]. Consequently, rudimentary genome-duplication "repair" systems were introduced that selected DNA over duplex RNA, thereby yielding a "reduced error" genome-duplication system. In this case, quantum processing information enzymes (QPIE) gradually expedited genomic evolution from (*i*) the era of pre-LUCA RNA "genome-like" polymers, (*ii*) to the "complete" duplex RNA genome, (*iii*) to the RNA-DNA reverse transcriptase genome, (*iv*) to double helical DNA genomes. These postulated four stages of pre-cellular genome evolution, and contents of their corresponding primordial pools, are schematically represented in Figure 9 (from Koonin et al. with permission) [66].

This model implies a form of Grover's-type [20] quantum information processing has been operational over the past ~ 3.6 or so billion y [16-19]. The quantum

reader was refined during the developmental era of duplex RNA genomes, and has been retained and "fine-tuned" for analogous operations in double helical DNA systems [16,35-37,51-53,59-61,63-66].

Consequently, accumulated entangled proton qubit states within ***G′-C′***, ****G-*C*** and ****A-*T*** sites of modern double helical DNA are "transparent" to the recently evolved DNA repair system, but are recognized and processed by the "earlier evolved" RNA system where enzyme-proton quantum entanglements implemented molecular clock, ***ts*** and ***td*** [1,16,17-19,44,51,89]. Soon after genome conversion from duplex RNA to double helical DNA [47,99], rates of *keto-amino* → *enol-imine* arrangement (Figure 3) responsible for ***ts*** were reduced by ~ 50- to 100-fold, because of 5-methyluracil (thymine) replacing uracil and cytosine replacing 5HMC [98]. This quantum-based evolutionary selection provided a "favorable" ***ts:td*** ratio, exhibited as *stochastic* random genetic drift for double helical DNA. Observation that rates ***ts*** ($\tau \approx 3200$ y) ≥ 1.5-fold ***td*** ($\tau \approx 6000$ y) implies a slight A-T richness, consistent with model prediction [17-18, 35-36,52-53,58]. Observable, *stochastic* random genetic drift is a consequence of EPR entanglement-enabled ***ts*** + ***td*** [16-19,52-53,58].

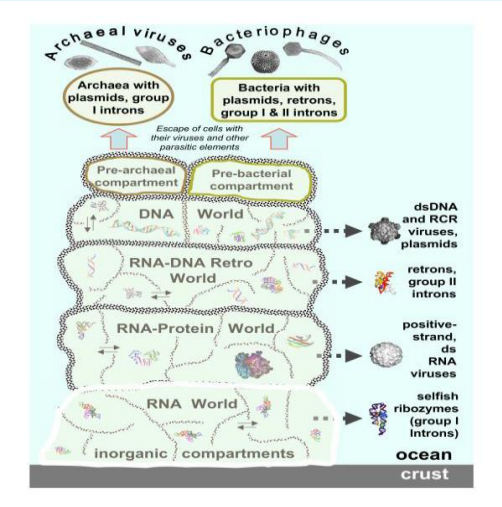

Figure 9. Evolution of genomic lineages from the primordial gene pool (from (Figure 2) with permission) [66]. Characteristic images of RNA and protein structures are shown for each postulated stage of evolution, and characteristic virion images are shown for emerging classes of viruses. Thin arrows show the postulated movement of genetic pools between inorganic compartments. Block arrows show the origin of different classes of viruses at different stages of pre-cellular evolution.)

A reverse-time extrapolation from observables exhibited by ancient T4 phage DNA implies that entangled proton qubits could have originally emerged in the first "susceptible" ancestral duplex segments of primitive RNA – ribozyme systems [35-36,63-66,98]. This assumption requires primordial ribozyme – RNA duplex segments to simulate, approximately, conditions exhibited by ancient T4 phage DNA systems that accumulate EPR-generated entangled proton qubits in metabolically inert (extracellular pH 7, 20 ^{0}C) base pair isomer superpositions, observed as ***G′-C′***, ****G-*C*** and ****A-*T*** [17-18,35-37]. This scenario provides a possible source of "RNA-type" hydrogen bonded duplex molecules susceptible to occupancy by EPR-generated entangled proton qubits [16-19,35-36], and thus, allowed ancestral peptide-ribozyme – RNA systems to form entanglement states with oscillating, $|+\rangle \rightleftarrows |-\rangle$, entangled proton qubits, occupying decoherence-free subspaces within hydrogen bonded duplex RNA segments [10-12,23-25,34,45,63-66,100]. At this stage of evolutionary development, peptide-ribozyme – proton entanglements could implement an entanglement-directed quantum search, $\Delta t' \leq 10^{-14}$ s < $\tau_D < 10^{-13}$ s to select the next amino acid electron lone-pair, or amino proton, to be added to the pre-protein peptide polymer [[1,5,16,31,47].

Additionally before proton decoherence, $\tau_D < 10^{-13}$ s, operations of the entangled ribozyme – proton system included (*a*) generating a transcribed message based on quantum informational content of "measured" entangled proton qubit-pairs (*b*) implementing an entanglement-directed quantum search, $\Delta t' \leq 10^{-14}$ s that specifies the incoming base's electron lone-pair, or amino proton, for evolutionary substitution, ***ts***, or deletion, ***td***, and (*c*) feedback responding — "Yes" or "No" — to *translation* of the transcribed "qubit message" [16-19,31,35-36]. "Yes" implies existence of an "*r+*-type" allele which allows replication initiation, but "No" identifies an unacceptable "mutant allele", *rII*, and therefore, replication is denied. Before "DNA-type" repair enzymes were introduced RNA – ribozyme systems avoided evolutionary extinction by disallowing conserved, "*rII*-type" allele contribution to the gene pool when "excessive" EPR-generated mutations (entangled qubits) were present [1, 16,35-36,47,89,100]. Other "relaxed" genes were allowed mutation, variation and selection. These processes introduced viable peptide-ribozyme – RNA, wild-type "*r+*-systems" where peptide-ribozyme – proton entanglements were exploited to generate rudimentary peptide chains that subsequently usurped ribozyme functions. When duplex RNA genomes became "too massive" for efficient, "error-free" duplication, "repair" enzymes were selected that

ultimately replaced RNA with DNA, thereby introducing DNA – protein systems [1-2,5,16,47,89,99].

Participation of EPR-generated entangled proton qubits eliminates the necessity of a Many Worlds in One (MWO) hypothesis for origin and existence of life on planet Earth. Koonin's classical assessments imply nascent DNA – protein systems ("biological evolution" in Figure 8) possess sufficient evolution potential to evolve into more complex living systems and organisms. In this case, Koonin's MWO hypothesis — that the probability of existence of any possible evolutionary scenario in an infinite multi verse is exactly 1 — is *not* required [5,16-19]. When EPR-generated entangled proton qubits are *not* ignored — as done in original studies of time-dependent evolution dynamics exhibited by (*i*) T4 phage DNA [35-37], (*ii*) age-related human cancer [19,42,77], (*iii*) rodent-human microsatellite distributions [17-18,21], (*iv*) Huntington's disease [16,44,59,61], etc. — the MWO hypothesis is not required to explain origin and evolution of life on an "Earth-like" planet in Earth's universe. The introduction of EPR-generated entangled proton qubits allows life-forming polymers to originate in an ancestral RNA – ribozyme system, where bio-molecular quantum processors simulate a "truncated" Grover's [20] quantum search to "measure" entangled proton qubit states, which provides a hypothesis for origin of the triplet code, utilizing 4^3 codons and ~ 22 L-amino acids. Consequently, ribozyme-peptide "processing" of entangled proton qubits could generate RNA – protein systems where "repair" enzymes ultimately intercede to replace unstable RNA with DNA [1,10-12,89]. Subsequent quantum entanglement algorithmic processing of entangled proton qubit-pairs allows DNA – protein systems to further evolve on Earth as observed and originate and evolve on other "Earth-like" planets in Earth's universe so, the MWO hypothesis is not required [1-5,16-19,51-53].

Genomic Growth via EPR-Generated "Dynamic Mutation"

Quantum informational content is introduced into *heteroduplex heterozygote* ***G′-C′*** and ****G-*C*** isomer pairs, and ****A-*T*** superpositions, by EPR-generated entangled proton qubit-pairs (Figures 1-4) — *keto-amino —(entanglement)→ enol–imine* — observed as, G-C → ***G´-C´***, G-C → ****G-*C,*** A-T →***A-*T*** [16-18]. *Entanglement-enabled* replication of ***G′-C′*** and ****G-*C*** yields ***ts,*** expressed as ***G′2 0 2 → T, G′0 0 2 → C, *G0 2 0⁰ → A*** & ****C2 0 2² → T*** (Tables 1 & 2) but *entanglement-enabled* replication of ****A-*T*** sites (Figure 4) exhibits time-dependent deletions, ***td***, i.e., ****A →*** deletion and ****T*** → deletion [17-18,35-36,44]. Observable EPR-generated entangled proton qubit state superpositions — ***G′-C′, *G-*C, *A-*T*** — are *not* recognized by "recently" evolved DNA repair systems, but *are* recognized and processed by enzyme-proton entanglement systems that evidently emerged in pre-LUCA (last universal cellular ancestor) RNA – ribozyme duplex segments [1,5,16-19,35-37, 42-44, 47,63-66, 77, 89].

Entangled proton qubits populating ancestral RNA duplex segments enabled peptide-ribozyme – proton entanglements the opportunity to "fabricate" polypeptides that ultimately replaced ribozyme function. Based on measured quantum informational content embodied within the 20 *available* entangled proton qubit states occupying ***G′-C′, *G-*C*** and ****A-*T*** superposition sites a rationale is implied for a "coding principle" that specified a redundant triplet genetic code of 4^3 codons for ~ 22 L-amino acids [5,16-19]. Within this context, a "truncated" Grover's [20] quantum search could simulate, approximately, bio-molecular quantum "measurements" of entangled proton qubit states, which implies a mechanism — Eq (15) — for selecting the triplet genetic code of 43 codons for ~ 22 L-amino acids. In this case, entanglement-enabled information processing introduced ***ts*** — ***G′2 0 2 →*** *U,* ***G′0 0 2 →*** *5HMC0⁰22²,* ***5HM*C2 0 22 →*** *U,* ****G0 2 0⁰ →*** *A* — and ***td, *A*** → deletion & ****T*** → deletion. Consistent with emergence of EPR-generated enzyme – proton entanglement processing in ancestral RNA an "evolved" quantum entanglement algorithm created ***ts*** and ***td*** in ancestral RNA and DNA genomes, which can introduce, and eliminate, initiation codons — UUG, CUG, AUG, GUG — and termination codons — UAA, UGA, UAG — thereby causing "dynamic mutations" that exhibit expansions and contractions[1-5,10-12, 16-19, ,44, 47, 59-62,63-66].

If genomic growth over the past ~ 3.5 billion years were consequences of entanglement-enabled ***ts*** + ***td*** introducing "dynamic mutations", "susceptible" microsatellite content in a genome would be proportional to genome size of the prokaryote or eukaryote organism, which *is* consistent with observation [16-19,21,47,59-61,101]. In duplex DNA of human genomes, unstable repeats exhibit expansions and contractions via "dynamic mutations", which in the case of (CAG)n sequences (n > 36), can exhibit expansions ≥ 10 (CAG) repeats in 20 y [16-19,44,59-62]. This observation implies the hypothesis that susceptible ancestral genomes implemented EPR-dependent, dynamic mutation expansions as consequences of effective ***ts*** + ***td***, introducing and eliminating, initiation and termination codons [16-19,44,47,59-61]. A "net" triplet repeat dynamic mutation expansion rate of 13 repeats, e.g., $(CAG)_{13}$ = 39 bp, per 20

y for 3.5 billion y would generate a genome of ~ 6.8×10^9 bp, which is "ballpark" compatible with bp content of the *Homo sapiens'* genome[16-19,44,59-61]. This explanation predicts that each organism's genomic growth will continue until a "stable" ***ts:td*** ratio is achieved. DNA genomes of T4 bacteriophage have evidently achieved this ***ts:td*** ratio stability[98]. Since rates, Σi d/dt(***tsi*** + ***tdi***), are a function of microsatellite availability, which can be increased, or eliminated, by ***ts*** and/or ***td***, a "stable" ***ts:td*** ratio has not been established for *H. sapiens'* eukaryotic genome; so, this entanglement-enabled evolution mechanism implies a rationale for origin and existence of "dynamic" CNGS [16-19,21, ,44, 59-60, 87-88].

Gatekeeper Gene's "Score Card" for "Tolerable" EPR-Generated Entangled Proton Qubits

Over the past ~ 3.5 or so billion years, pre-cellular prokaryotic and eukaryotic evolution had ample opportunity to select preferable, advantageous mechanisms for protecting the gene pool, and conserved noncoding genomic spaces (CNGS) against acquiring *unsafe* levels of entangled proton qubits in haploid and diploid genomes [1,2,18-19,35-37,42,47,51-53,59-61,63-66,77,97,87,88]. Although DNA repair enzymes were acquired during transitions from ancestral RNA to DNA genomes [1,5,16,47,66,89,99], the originally selected quantum entanglement algorithm for RNA genomic evolution (Figure 8) was retained, and further refined, for entanglement-originated ***ts*** and ***td*** in DNA systems. Consequently, *all* phases of haploid and diploid genomic DNA evolution — precellular, prokaryotic, eukaryotic — were successfully executed under conditions of continuous accumulations of EPR-generated entangled proton qubits, subsequently deciphered by enzyme – proton entanglements to yield ***ts*** and ***td***, exhibited as ***SNPs*** that enabled "dynamic mutation" expansions [5,16-19,20,44,47,52-53,59]. The evolutionarily selected, continuous acquisition of EPR-generated entangled proton qubits implies necessity of an evolutionary mechanism that "protects" against consequences of "unchecked" accumulations of entangled proton qubits, which would be "unsafe" if contributed to the gene pool [16-19,35-36,42-43].

Consistent with observation and theory, a sensitive CNGS, *s,* for *Homo sapiens* can be defined by the inequality, $1 \geq s \geq 0.97$ [10-12,16,18-20,35-36,42-45,87-88]. This inequality is based on ~100 y as the maximally allowed *Homo sapiens'* age, and experimental measurements of mean lifetimes, τ, for metastable keto-amino G-C states in genomic DNA (37^0C; pH 7), $\tau \geq 3000$ y [35-36,44]. Thus, at age 100 y, ~ 3% (100/3000x100) of G-C sites in the *Homo sapiens'* genome would have been populated by EPR-generated, entangled proton qubit arrangements, *keto-amino → enol-imine,* via the symmetric and asymmetric channels, G-C → ***G′-C′*** and G-C → ****G-*C*** (Figures 1-4). Subsequent enzyme – proton entanglement processing (Table 1) introduces ***ts*** (and ***td*** at ****A-*T*** pairs). Accordingly, robust *Homo sapiens* infants inherit normal "wild type" CNGS inequality, $1 \geq s \geq 0.97$. EPR-generated entangled proton qubits provide entanglement-enabled mechanisms for mutation, variation, selection and genome growth, until proton qubit accumulation satisfies the "threshold condition", $s \approx 0.97 + \epsilon$, generally at an advanced age (Figure 7).

When EPR-generated entangled proton qubits satisfy the "threshold condition" — $s \approx 0.97 + \varepsilon$ — the probability is significantly enhanced that the subsequent round of ***ts*** + ***td*** will express selected ***SNP*** mutant proteins responsible for elimination of haploid genomes [16-19,42-44,77-80,82,92]. In these cases, conserved "gatekeeper" genes are eliminated by spermatogenesis or oogenesis in the haploid state, but manifest an age-related degenerative disease in the diploid state [16-19]. If conserved "gatekeeper" genes had been populated to the threshold limit, i.e., to $s \approx 0.97 + \varepsilon$, *and* were then contributed to the gene pool, rapid evolutionary extinction would ensue [16,36,44,90]. Consequently, "unsafe" haploid genomes are eliminated during spermatogenesis and oogenesis, thereby preserving "wild type" gene pool viabilities, and enabling species survival [16]. However diploid genomes populated to "unsafe" threshold limits, $s \approx 0.97 + \varepsilon$, encounter discrimination by conserved "gatekeeper" genes e.g., "cancer genes", "Alzheimer's genes" the *huntingtin* gene "ALS genes" the progeria gene and "other" genes [16-19,61-62, 76-80,82-85,94-95,102-103]. In these cases, ***ts + td*** introduce specific ***SNPs*** which cause manifestation of the respective age-related degenerative disease [16,18-19,42-44].

An example of "gatekeeper" genes' operational mechanism is provide by a quantum entanglement algorithm explanation of haploid human oocytes' function – normal menopause – in terms of Orgel's "error catastrophe" hypothesis. Routine EPR-generated entangled proton qubits introduce mutation, variation and selection in terms of entanglement-enabled ***SNPs*** [16,18-19,104,105]. However, when CNGS, s ($1 \geq s \geq 0.97 + \epsilon$), of "gatekeeper" genes acquire EPR-generated entangled proton qubits to their "threshold limit", i.e., to $s \approx 0.97 + \varepsilon$, such "evolutionarily depleted" genes are disallowed contributions to the gene pool, due to selected, EPR-generated "error catastrophe" criteria [10-12,16-19,105].

Internal female oocytes operate in 37 ^{0}C environments, but "external" male haploid genomes are in environments of reduced temperature, ~ 34^0 C [106]. Vibrational modes in the DNA double helix are more energetic at 37 ^{0}C than at ~ 34^0 C; so, more energetic vibrational modes would increase probabilities of quantum uncertainty limits, $\Delta x\ \Delta px \geq \hbar/2$, operating on metastable amino ($-NH_2$) protons, which generate EPR arrangements, *keto-amino* → *enol-imine* (see Appendix) [107-108]. Consequently, observed rates of accumulating entangled proton qubit-pairs are ~ 3-fold greater in 37 ^{0}C oocyte DNA than in ~ 34 ^{0}C sperm [36,106-107]. Therefore, evolutionarily selected thresholds, s ($1 \geq s \geq 0.97 + \epsilon$), in CNGS of oocytes are populated — to the "threshold limit", $s \approx 0.97 + \epsilon$ — at ~ 3-fold enhanced rates for EPR-generated entangled proton qubits, compared to EPR-qubit rates in ~ 34 ^{0}C sperm DNA [42-43,106]. When the "threshold limit" s-value is attained, $s \approx 0.97 + \epsilon$, the haploid oocyte CNGS has been "evolutionarily depleted" by its acquired limit of EPR-generated entangled proton qubits [16,18,19]. Such "unsafe" haploid genomes are evolutionarily disallowed contribution to the gene pool by menopause [104]. This prevents "unsafe" contamination of the gene pool, which enables species' survival at the expense of sacrificing an "operational", but evolutionarily depleted, host genome [1,16,42-44]. In this case, normal human menopause is implemented by "gatekeeper" genes that disallow haploid genomes — containing "unsafe" levels of EPR-generated entangled proton qubits — from contributions to the gene pool [16,18-19,104]. This allows the "gene pool" to retain an approximately "wild-type" spectrum of conserved genes that exhibit age-related disease as consequences of EPR-generated ***SNP*** [16,18-19,92]. Evidently this temperature-dependent, ~ 3 to 4 ^{0}C, haploid selection of female genomes has provided female *H. sapiens* with a slightly longer life-span than males [104].

"Gatekeeper" genes preserve "wild type" gene pool viability and enable species' survival by eliminating – from the gene pool – evolutionarily depleted, "unsafe" genomes. Operational functions of "gatekeeper" genes provide a quantum entanglement version of Orgel's "error catastrophe" hypothesis. In this case, quantum uncertainty limits, $\Delta x\ \Delta p_x \geq \hbar/2$, operate on hydrogen bonding amino protons to introduce EPR-generated entangled proton qubits. When CNGS, s ($1 \geq s \geq 0.97$), of "gatekeeper" genes acquire entangled proton qubits to their "threshold limits", i.e., to $s \approx 0.97 + \varepsilon$, such genes are disallowed contributions to the gene pool, due to "excessive" EPR-generated entangled proton qubits viewed classically as "error catastrophe" criteria [16-19,77-80,82-85,104,105].

Classical evolution theory claims that natural "purifying" selection would eliminate deleterious genes that accumulate "unsafe" entangled proton qubits, including "cancer genes", "Alzheimer's genes", the *huntingtin* gene, the progeria gene, "ALS genes" (amyotrophic lateral sclerosis) and "other" genes, which did *not* happen. Rather these evolutionarily conserved "beneficial genes" have been retained to execute their *necessary* "gatekeeper" functions of disallowing contributions to the gene pool by genomes that have acquired EPR-generated entangled proton qubits to "unsafe" levels, i.e., to $s \approx 0.97 + \epsilon$ [16,18-19,42-44,47,52-53,61-62,76-80,82-85,92,94,95,102-104,109-110]. This prevents "unsafe" contamination of the gene pool by excessive EPR-generated entangled proton qubits, which enables species' survival at the expense of sacrificing "operational", but evolutionarily depleted, host genomes [16-19,104].

Discussion and Conclusion

Studies of entanglement-enabled information processing require the most fundamental theory of matter — quantum theory — to understand and explain EPR-generated entangled proton qubit reactive processes, exhibited by evolving duplex DNA systems [1-2,10-12,13-19,21,33,35-36,41-44,51,54-56,61,75,77,82]. Since appropriately challenged predictions of quantum theory have *never* been wrong, entanglement-enabled predictions, and biological consequences, of EPR-generated entangled proton qubits are susceptible to the very powerful analytical tools and assessments of quantum information theory [1-2,8,10-12,16-20,33,41-45,54-56]. Within this context, and consistent with quantum approximations in the Appendix, Eq (22) provides valid approximations for classical, $\Sigma i\lambda it^3$, and EPR-generated entangled proton qubits' contributions, $\Sigma_j\beta_j t^4$, to genetic information responsible for manifestation of an age-related disease[16,18-19]. In cases Huntington's disease an "expanded" $(CAG)n$ ($n \geq 36$) repeat is inherited where its enigmatic molecular evolutionary dynamics are described by quantum entanglement terms, $\Sigma_j\beta_j t^4$, in Eq (22) [16,19,44,61].

(Figure 10) illustrates the phenomenon of genetic *anticipation* where earlier disease onset is exhibited in progeny that inherit longer, "expanded" $(CAG)n$ repeats, i.e., $n > 36$ [59-62]. When $n \geq 70$, phenotypic manifestation of disease is delayed ~2 to ~12 y after birth (Figure 10), but for $n < \sim 36$ disease is not expressed in that generation [61]. Classical Watson-Crick transcription and replication of inherited $(CAG)_{70}$ repeats would yield phenotypic expression within hrs., days or weeks after

birth, not delays of ~2 to ~12 y before Huntington's disease is manifested [47]. This ~2 to ~12 y delay is explained as the time required for the $(CAG)_{70}$ "threshold limit" to be populated with EPR-generated entangled proton qubits, *keto-amino* → *enol-imine* [16,91]. In this case, phenotypic expression is a consequence of "measured" quantum information content within EPR-generated entangled proton qubits occupying a "threshold limit" of the inherited $(CAG)_{70}$ repeat [16,44]. This explanation is also applicable to congenital myotonic dystrophy, where inherited (CTG)n (n ≥ 750) repeats manifest disease ~ 12 months after birth[93].

In these cases, EPR-proton qubits participate in entangled quantum oscillations, ~ 4×10^{13} s^{-1}, between near-symmetric energy wells in decoherence-free subspaces of enol oxygen and imine nitrogen [16-19,23-25]. The resulting "ground state collapse" structure of double helical DNA base pairs, occupied by "stable" EPR-generated entangled proton qubits is bound more tightly by ~3 to ~7 Kcal/mole and predicts a less flexible double helix, exemplified by "breakage" of Fragile X (CCG)n-repeats, occupied by EPR-proton qubits [16,17-18,36,59-60]. Observables exhibited in Figure 10 are consequences of Grover's processors quantifying the smallest "measurable" genetic informational unit – entangled proton "qubit-pairs" – which specifies quantum information processing instructions to manifest phenotypic expression [16,19].

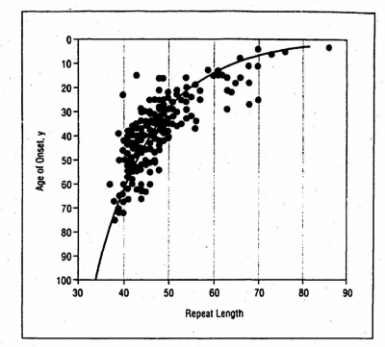

Figure 10: (CAG)n repeat length versus age-of-onset of Huntington's disease (adapted from (Figure 3) of [61].

Long-term stability of EPR-generated entangled proton qubit-pairs allows evolutionary distributions of the 22 most abundant microsatellites common to rat and human to be specified by Grover's processors measuring, $\delta t << 10^{-13}$ s, quantum informational content of EPR-generated entangled proton qubits [16-20,21]. In these cases, Grover's-type [20] quantum processor "crawls" along major and minor genome grooves at ~ 10^{-5} cm s^{-1}, where it "quantifies" quantum informational content of entangled proton qubit superpositions, $|+> \rightleftarrows |->$, oscillating in decoherence-free subspaces, between near symmetric energy wells at ~ $4x10^{13}$ s^{-1}[23-25, 38,45,48-49]. In intervals, $\delta t << 10^{-13}$ s, Grover's processor "traps" an entangled-state proton, $|->$, in a major or minor groove (Table 1), which creates an enzyme – proton entanglement. Before proton decoherence — $\Delta t' \leq 10^{-14}$ s < τ_D — the enzyme – proton entanglement implements quantum information processing (Table 1), which specifies evolutionary distributions of, for example, rat and human microsatellites [17-18,21]. Therefore, consistent with observation and analyses, neither water, ionic incursions or random temperature fluctuations obstruct quantum information processing, $\Delta t' \leq 10^{-14}$ s < τ_D, executed by rat and human genomes [17-18,21,31,54-56,67]. Quantum information processing algorithms are analogously operational in DNA of human brain-cells, which are embedded within an evolutionarily selected neural circuitry [7-9,16-19,44,68-70]. Consequently, quantum information processing, $\Delta t' \leq 10^{-14}$ s, of EPR-generated entangled proton qubits, executed by a single brain-cell, could communicate the resulting quantum information processing calculations to the brain's neuronal network of ~ billons of neurons [16-19,54-56,68-70]. This evolutionarily coordinated "network" communication could cause entanglement-enabled information-processing computations in ~ billons of brain-cell DNA systems, and consequently, execute the phenomenon of consciousness [7-9,68].

Since several dominant concepts in contemporary neuroscience were developed approximately ~ 50 to 100 years ago, Stern recently suggested that "proper" interpretation of observation, and construction of theoretical models, could benefit from "updated concepts" [68]. To this end, a consideration of neuroscience research "big questions" was reviewed, e.g., consciousness neuroscience industrialization, "proper" animal models in neuroscience, "microscopic" brain processes in prefrontal cortex, and space – time concepts within brain tissue [7,70,111-113]. Frégnae argues that enhanced interdisciplinary collaboration between physics and biology would yield greater resolution and insight into information processing by neurological cells, which agrees with and this report [7,70].

Based on recent studies, quantum information processing of EPR-generated entangled proton qubit-pairs *is* operational in *all* duplex DNA systems [1-2,10-19,35-37,42-44,51-*56*,60-61]. In this case, quantum-level

resolution — e.g., identification of selected and rejected eigenstates constituting a "measured" superposition system in (Table 1)— becomes available for biochemical studies of cognitive processes, at the level of an entangled proton qubit, "trapped" in a genome groove [38]. Empirical evidence implies that consciousness can originate from specific computations; so, quantum information processing by brain-cell DNA suggests an evolutionarily selected entanglement-enabled "working hypothesis" for consciousness, executed within the neural circuitry network of brain-cell DNA systems [7-9,16-19,54-56,68-70,112]. In these cases, quantum information processing, $\Delta t' \leq 10^{-14}$ s, implemented by a single human brain cell could communicate the resulting quantum information processing calculations to the brain's neuronal network of ~ billons of neurons [7,16-19,54-56,68-70,112]. Analogous to evolution instructions provided by "measured" quantum informational content embodied within EPR-generated entangled proton qubit-pairs orchestrated quantum information processing of entangled proton qubit-pairs in brain cell DNA could be responsible for the phenomenon of human consciousness [7-9,16 -19,21,44,68-70,111-113].

Avenues for neuroscientists to investigate properties of EPR-generated entangled proton qubit-pairs are provided, e.g., by Huntington's disease patients with "long" inherited (CAG)n (n ≥ 37) repeats [16,44,59,61-62]. The time between birth and manifestation of Huntington's disease is the time required for EPR-generated entangled proton qubits to populate the inherited (CAG)n to its "threshold limit" [16,61]. In these cases, phenotypic manifestation of Huntington's disease *requires* Grover's [20] processors to measure quantum informational content — embodied within EPR-generated entangled proton qubits — that occupies the (CAG)n-repeat to its "threshold limit". This observation (Figure 10) can be exploited to investigate quantum information processing of EPR-generated entangled proton qubit-pairs in brain-cell DNA [10-12,16,-19,54-56,61]. Huntington's disease provides an example malfunction of quantum information processing of EPR-generated entangled proton qubits in neurological cells. However, "properly implemented" quantum information processing of EPR-generated entangled proton qubits in brain-cell DNA could, this report argues, participate in cognitive processes responsible for consciousness [7-9,16,18, 44,68-70].

The "long-term" availability of EPR-generated entangled proton qubit-pairs provided additional entanglement-enabled information processing options — not accessible to classical evolution mechanisms — on which Darwinian selection operates to generate more advantageous and versatile biological functions [1-9,16-21,47,51-56,58-61,63-66,77,82]. Recognition of EPR-generated entangled proton qubit-pairs' role in evolution identifies "new", quantum-level insight into responsible mechanisms, and their consequences [16-19]. These includes an entanglement-enabled information processing mechanism for consciousness, existence of "gatekeeper genes", genome growth in terms of EPR-generated "dynamic mutations" and a quantum entanglement model for origin of the genetic code, where 4^3 codons specify ~ 22 L-amino acids [1, 7,16-19,44,59-61].

Based on recent studies, EPR-generated entangled proton qubit-pairs *must retain* entangled "two-state" quantum coherence, $|+> \rightleftarrows |->$, *for years to decades*, before specifying microsatellite evolution instructions with "measured" quantum informational content of EPR-generated entangled proton qubit-pairs [1-2,16-19,21]. Dynamic, "intra-atomic", EPR-generated entangled proton qubit states are resistant to decoherence by "normal" *in vivo* classical environments, but are evolutionarily selected to communicate quantum informational content when "measured", $\delta t << 10^{-13}$ s, in state $|->$ within a genome groove [38], by Grover's [20] enzyme quantum reader (Table 1) [17-19,26-30,44-45,47,51,54-56,67]. Stability of EPR-generated entangled proton qubits is explained by their "intra-atomic", quantum-dynamic two-state, $|+> \rightleftarrows |->$, entangled oscillations at ~ $4x10^{13}$ s^{-1}, within decoherence-free subspaces of enol oxygen and imine nitrogen. This report argues that stability of EPR-generated entangled proton qubits allows entangled proton qubit-pairs to function as "quantum informational-reservoirs" that are measured by Grover's [20] processors, and thus, are responsible for quantum information processing instructions that implement human consciousness [7-9,13-21,23-25,45]. This hypothesis is supported by evidence that EPR-generated entangled proton qubits are responsible for "gatekeeper genes", which implies their participation in age-related Huntington's disease and age-related ALS [16,18-19,44,61,94-95].

In any case, recent studies [16-19] provide "fresh views"– looking through a "quantum lens" – in efforts to explain EPR-generated entangled proton qubits observed, for example, as enigmatic data exhibited by Huntington's disease [59,61,] and age-related cancer incidence, (Figure 7) [42,77]. Availability of EPR-generated entangled proton qubits — for quantum information processing — appears to be applicable in manifestation of these maladies; so, this report argues, that analogous EPR-originated, entanglement-enabled information processing

may be responsible for executing reactive processes that exhibit human consciousness [6-9,16-19,54-56,68-70,111-113]. Finally, quantum entanglement phenomena — EPR-generated entangled proton qubits in biological systems — *cannot* be effectively studied using "classical-only" methods [55,61,67,75,77]. But implementation of realistic, "quantum-level" treatments of EPR-generated entangled proton qubits, and their evolutionary consequences, will benefit future progress in resolving certain "obstinate" age-related disease questions [16-19,61,75,77-86,94]. These recent studies are consistent with prior views of Delbrück, Schrödinger and Löwdin that quantum phenomena play significant roles in governing dynamics of time-dependent evolution of genetic information [16-19,114-117].

Acknowledgements

I thank Roy Frieden for useful discussions on quantum coherence and decoherence of enzyme – proton entanglements in biological systems. Don Kouri and John Sabin provided helpful comments on this research which are appreciated. Discussions with Peggie Price and Peggy Johnson on origins of human consciousness provided motivation to write this manuscript. The author states that no conflicts of interests exist to declare.

References

1. Cooper WG (2016) Quantum information processing model explains "early" and "recent" genome repair mechanisms. Res Reviews J of Pure Applied Physics 4(2): 74-100.

2. WG Cooper (2018) Origin of Life Insight: Reactive Transitions from Anthropic Causality to Biological Evolution. OMICS Group e-Books.

3. Caleb Scharf, Nathaniel Virgo, James C, Masashi A, Nathanael AK, et al. (2015) Strategies for origins of life research. Astrobiol 15(12): 1031-1042.

4. Benner SA (2014) Paradoxes in the origin of life. Orig. Life Evol Biosph 44(4): 339-343.

5. Koonin EV (2012) The Logic of Chance. The Nature and Origin of Biological Evolution. Pearson, FT Press. Upper Saddle River, New Jersey.

6. Fleming GR, Scholes GD (2014) Quantum Biology: Introduction. In: Mohseni M, Omar Y, Engel GS, Plenio MB, (Eds.), Quantum Effects in Biology. Cambridge University Press, Cambridge, UK, pp: 3-13.

7. Dehaene S, Lau H, Kouider S (2017) What is consciousness and could machines have it? Science 358(6362): 486-492.

8. Rosenblum B, Kuttner F (2011) Quantum Enigma: Physics Encounters Consciousness. 2nd (Edn.), Oxford University Press, New York.

9. Hameroff S, Penrose R (2014) Consciousness in the universe: a review of the "Orch OR" theory. Physics of Life Reviews 11(1): 39-78.

10. Einstein A, Podolsky B, Rosen N (1935) Can Quantum Mechanical Description of Physical Reality be Considered Complete? Phy Rev 47: 777-780.

11. Schrödinger E, Born M (1935) Discussion of probability relations between separated systems. Mathematical Proceedings Cambridge Philosophical Society 31(4): 555-563.

12. Schrödinger E, Dirac PAM (1936) Probability relations between separated systems. Mathematical Proceedings Cambridge Philosophical Society 32(3): 446-452.

13. Horodecki R, Horodecki P, Horodecki M, Horodecki K (2009) Quantum entanglement. Rev. Mod Phys 81: 865-942.

14. De Vicente JI, Spee C, Kraus B (2013) Maximally entangled set of multipartite quantum states. Phys Rev Lett 111: 110502.

15. Pfaff W, Taminiau TH, Robledo L, Bemien H, Markham M, et al. (2013) Demonstration of entanglement-by-measurement of solid-state qubits. Nature Physics 9: 29-33.

16. Cooper WG (2016) Molecular dynamics responsible for observable Huntington's disease $(CAG)_n$ repeat evolution. Ann Neurodegener Dis 1(2): 1009.

17. Cooper WG (2017) Evolution via EPR-entanglement algorithm execution. J Biomed Engr Med Imag 4(2): 43-95.

18. Cooper WG (2017) EPR–proton qubits' role in evolution and age-related disease. Phys Sci Biophys J 1(1): 000104.

19. Cooper WG (2018) Consequences of EPR–proton qubits populating DNA. Adv Quantum Chem 77: 19-120.

20. Grover LK (1996) A fast quantum mechanical algorithm for database search. In: Proc. 28th Annual ACM STOC ACM Philadelphia: 212-219.

21. Beckmann JW, Weber JL (1992) Survey of human and rat microsatellites. Genomics 12(4): 627-631.

22. Kumar S, Hedges, SB (1998) A molecular timescale for vertebrate evolution. Nature 392(6679): 917-920.

23. Xu GF, Zhang J, Tong DM, Sjöqvist E, Kwek LC (2012) Nonadiabatic holonomic quantum computation in decoherence-free subspaces. Phys Rev Lett 109: 170501.

24. Xu G, Long G (2014) Universal nonadiabatic geometric gates in two-qubit decoherence-free subspaces. Sci Rep 4: 6814.

25. Suter D, Álvarez GA (2016) Protecting quantum information against environmental noise. Rev Mod Phys 88: 041001.

26. Arndt M, Juffmann T, Vedral V (2009) Quantum physics meets biology. HFSP J 3(6): 386-400.

27. Wiseman HM, Eisert J (2008) Nontrivial quantum effects in biology: A skeptical physicist's view. In: Abbott D, Davies PCW, Pati AK (Eds.), Quantum Aspects of Life. Imperial College Press, London, pp: 381-402.

28. McKemmish LK, Riemers JR, McKenzie RH, Hush NS (2009) Penrose-Hameroff orchestrated objective-reduction proposal for human consciousness is not biologically feasible. Phys Rev E 80(2 pt 1): 021912.

29. Lambert N, Chen YN, Cheng YC, Li CM, Chen GY, et al. (2013) Quantum biology. Nature Phys 9: 10-18.

30. Tamulis A, Grigalavicius M (2014) Quantum entanglement in photoactive prebiotic systems. Syst Synth Biol 8(2): 117-140.

31. Tegmark M (2000) The importance of quantum decoherence in brain processes. Phys Rev E 61: 4194-4206.

32. Kouri DJ (2014) Harmonic oscillators, Heisenberg's uncertainty principle and simultaneous measurement precision for position and momentum.

33. Merzbacher E (1997) Quantum Mechanics, John Wiley & Sons. 3rd (Edn.), New York.

34. Scheiner S (1997) Hydrogen Bonding. A Theoretical Perspective. Oxford University Press, Oxford.

35. Cooper WG (2009) Necessity of quantum coherence to account for the spectrum of time-dependent mutations exhibited by bacteriophage T4. Biochem Genet 47: 892.

36. Cooper WG (2009) Evidence for transcriptase quantum processing implies entanglement and decoherence of superposition proton states. Bio Systems 979(2): 73-89.

37. Ripley LS (1988) Estimation of in-vivo miscoding rates. Quantitative behavior of two classes of heat-induced DNA lesions. J Mol Biol 202(1): 17-34.

38. Wing R, Drew H, Takano T, Broka C, Tanaka S, et al. (1980) Crystal structure analysis of a complete turn of B-DNA. Nature 287: 755-756.

39. Feynman RP, Leighton RB, Sands M (1965) The Feynman Lectures on Physics. 3rd (Vol), Addison-Wesley, New York.

40. Bell JS (1964) On the Einstein-Podolsky-Rosen Paradox. Phys Ther 1(3): 195-200.

41. Bell JS (1993) Speakable and Unspeakable in Quantum Mechanics. Cambridge University Press.

42. Cooper WG (2011) Accuracy in biological information technology involves enzymatic quantum processing and entanglement of decohered isomers. Information 2(1): 166-194.

43. Cooper WG (2011) The molecular clock in terms of quantum information processing of coherent states, entanglement and replication of evolutionarily selected decohered isomers. Interdiscip Sci 3(2): 91-109.

44. Cooper WG (2012) Coherent states as consequences of keto-amino → enol-imine hydrogen bond arrangements driven by quantum uncertainty limits on amino DNA protons. Int J Quantum Chem 112(10): 2301-2323.

45. Monz T, Kim K, Villar AS, Schindler P, Chwalla M, et al. (2009) Realization of universal ion-trap quantum computation with decoherence free qubits. Phys Rev Lett 103: 200503.

46. Tegmark M, Wheeler JA (2003) 100 years of the Quantum. Sci Am 284: 68-75.

47. Watson J, Baker T, Bell S (2013) Molecular Biology of the Gene. 7th (Edn), Menlo Park, CA: Benjamin-Cummings.

48. Davies PCW (2004) Does quantum mechanics play a non-trivial role in life? Bio Systems 78(1-3): 69-79.

49. Goel A, Astumian RD, Herschbach D (2003) Tuning and switching a DNA polymerase motor with mechanical tension. Proc Natl Acad Sci USA 100(17): 9699-9704.

50. Wigner EP (1957) Relativistic invariance and quantum phenomena. Rev Mod Phys 29: 255-268.

51. Hwang DG, Green P (2004) Bayesian Markov chain Monte Carlo sequence analysis reveals varying neutral substitution patterns in mammalian evolution. Proc Natl Acad Sci USA 101(39): 13994-14001.

52. Kumar S (2005) Molecular clocks: four decades of evolution. Nat Rev Genet 6(8): 654-662.

53. Bromham L, Penny D (2003) The modern molecular clock. Nat Rev Genet 4(3): 216-224.

54. Zoller P, Beth T, Binosi D, Blatt R, Briegel H, et al. (2005) Quantum information processing and communication. European Physical J D 36(2): 203-228.

55. Vedral V (2006) Introduction to Quantum Information Science. Oxford University Press, UK.

56. Wilde MM (2013) Quantum Information Theory. Cambridge University Press, Cambridge.

57. Topal MD, Fresco JR (1976) Complementary base pairing and the origin of base substitutions. Nature 263: 285-289.

58. Whitney KD, Garland T (2010) Did genetic drift drive increases in genome complexity? PLoS Genet 6(8): e1001080.

59. Richards R (2001) Dynamic mutations: a decade of unstable expanded repeats in human genetic disease. Mol Hum Genet 10(20): 2187-2194.

60. Cooper WG (1995) Evolutionary origin of expandable G-C rich triplet repeat DNA sequences. Biochem Genet 33(5-6): 173-181.

61. Gusella JF, MacDonald ME, Ambrose CM, Duyao MP (1993) Molecular genetics of Huntington's disease. Arch Neurol 50(11): 1157-1163.

62. Semaka A, Creighton S, Warby S, Hayden MR (2006) Predictive testing for Huntington's disease: interpretation and significance of intermediate alleles. Clin Genet 70(4): 283-294.

63. Cech TR (2012) The RNA World in Context. Cold Spring Harbor Perspectives in Biology 4(7): a006742.

64. Shelke SA, Piccirilli JA (2014) Origins of life: RNA made its own mirror image. Nature 515(7527): 347-348.

65. Noller HF (2012) Evolution of protein synthesis from an RNA world. Cold Spring Harb Perspect Biol 4(4): a003681.

66. Koonin EV, Senkevich T, Dolja VV (2006) The ancient virus world and the evolution of cells. Biol Direct 1: 29.

67. Reif F (1965) Fundamentals of Statistical and Thermal Physics. McGraw Hill, New York.

68. Stern P (2017) Neuroscience in search of new concepts. Science 358(6362): 464-465.

69. Donato F (2017) Assembling the brain from deep within. Science 358(6362): 456-457.

70. Fregnae Y (2017) Big data and the industrialization of neuroscience: A safe roadmap for understanding the brain. Science 358(6362): 470-477.

71. Muller HJ (1950) Our load of mutations. Am J Hum Genet 2(2): 111-176.

72. Little MP (2010) Cancer models, genomic instability and somatic cellular Darwinian evolution. Biol Direct 5: 19.

73. Foo J, Leder K, Michor F (2011) Stochastic dynamics of cancer initiation. Phys Biol 8(1): 015002.

74. Feder T (2010) Physicists invited to apply their insights to cancer. Phys Today 63(5): 27-28.

75. Moore NM, Kuhn NZ, Hanlon SE, Lee JSH, Nagahara LA (2011) De-convoluting cancer's complexity: using a 'physical sciences lens' to provide a different (clearer) perspective of cancer. Phys Biol 8(1): 010302.

76. Weinberg RA (2013) The Biology of Cancer. 2nd (Edn.), Garland Science, New York.

77. Dix D, Cohen P, Flannery J (1980) On the role of aging in cancer incidence. J Theoret Biol 83(1): 163-171.

78. Bozic I, Antal T, Ohtsuki H, Carter H, Kim D, et al. (2010) Accumulation of driver and passenger mutations during tumor progression. Proc Natl Acad Sci 107(43): 18545-18550.

79. Illingworth CJR, Mustonen V (2011) Distinguishing driver and passenger mutations in an evolutionary history categorized by inference. Genetics 189(3): 989-1000.

80. Beerenwinkel N, Antal T, Dingli D, Traulsen A, Kinzler KW, et al. (2007) Genetic progression and the waiting time to cancer. PLoS Comput Biol 3(11): e225.

81. Anderson WF, Camargo MC, Fraumeni JF, Correa P, Rosenberg PS, et al. (2010) Age-specific trends in incidence of noncardia gastric cancer in US adults. JAMA 303(17): 1723-1728.

82. Cruchaga C, Haller G, Chakraverty S, Mayo K, Vallania FLM, et al. (2012) Rare variants in APP, PSEN1 and PSEN2 increase risk for AD in late-onset Alzheimer's disease families. PLoS One 7(2): e31039.

83. Sisodia SS, Tanz RE (2007) Alzheimer's disease: Advances in Genetics, Molecular and Cellular Biology, Springer Science + Business Media, New York.

84. Pifer PM, Yates EA, Legleiter J (2011) Point mutations in Aβ result in the formation of distinct polymorph aggregates in the presence of lipid bilayers, PLos One 6(1): e16248.

85. Mosconi L, Rinne JO, Tsui WH, Berti V, Li Y, et al. (2010) Increased fibrillar amyloid-β burden in normal individuals with a family history of late-onset Alzheimer's. Proc Natl Acad Sci USA 107(13): 5949-5954.

86. Qui C, Kivipelto M, von Strauss E (2009) Epidemiology of Alzheimer's disease: occurrence, determinants, and strategies toward intervention. Dialogues Clin Neurosci 11(2): 111-128.

87. Lujambio A, Portela A, Liz J, Melo SA, Rossi S, et al. (2010) CpG island hypermethylation-associated silencing of non-coding RNAs transcribed from ultra conserved regions in human cancer. Oncogene 29(48): 6390-6401.

88. Huang Y, Shen XJ, Zou Q, Wang SP, Tang SM, et al. (2011) Biological functions of microRNAs: A review. J Physiol Biochem 67(1): 129-139.

89. O'Brien PJ (2006) Catalytic promiscuity and the divergent evolution of DNA repair enzymes. Chem Rev 106(2): 720-752.

90. Cooper WG (1996) Hypothesis on a causal link between EMF and an evolutionary class of cancer and spontaneous abortion. Cancer Biochem Biophys 15(3): 151-170.

91. Wootters WK, Zurek WH (1982) A single quantum state cannot be cloned. Nature 299: 802-803.

92. Cooper DN, Youssoufian H (1988) The CpG dinucleotide and human genetic diseases. Hum Genet 78(2): 151-155.

93. Harper PS (2009) Myotonic Dystrophy. 2nd (Edn.), Oxford University Press, Oxford UK.

94. Dejesus-Hernandez M, Mackenzie IR, Boeve BF, Boxer AL, Baker M, et al. (2011) Expanded GGGGCC hexanucleotide repeats in noncoding region of C9ORF72 causes chrosome 9p-linked FTD and ALS. Neuron 72(2): 245-256.

95. Majounie E, Reton AE, Mok K, Dopper EG, Wait A, et al. (2012) Frequency of the C9ORF72 hexanucleotide repeat expansion in patients with amyotrophic lateral sclerosis and frontotemporal dementia: a cross-sectional study. Lancet Neurology 11(4): 323-330.

96. Hameroff SR (2006) The entwined mysteries of anesthesia and consciousness - is there a common underlying mechanism? Anesthesiology 105(2): 400-412.

97. Nutman AP, Bennett VC, Friend CRL, Van Kranendonk MJ, Chivas AR (2016) Rapid emergence of life shown by discovery of 3,700-million-year-old microbial structures. Nature 537: 535-538.

98. Miller ES, Kutter E, Mosig G, Arisaka F, Kunisawa T, et al. (2003) Bacteriophage T4 genome. Microbiol Mol Biol Rev 67(1): 86-156.

99. Takeuchi N, Hogeweg P, Koonin EV (2011) On the origin of DNA genomes: Evolution of the division of labor between template and catalyst in model

replicator systems. PLoS Comput Biol 7(3): e2002024.

100. Domingo E, Escarmis C, Sevilla N, Moya A, Elena SF, et al. (1996) Basic concepts in RNA virus evolution. FASEB J 10(8): 859-864.

101. Hancock JM (1996) Simple sequences and the expanding genome. Bio Essays 18(5): 421-425.

102. Gordon LB, Cao K, Collins FS (2012) Progeria: Translational insights from cell biology. J Cell Biol 199(1): 9-13.

103. Eriksson M, Brown WT, Gordon LB, Glynn MW, Singer J, et al. (2003) Recurrent de novo point mutations in lamin A cause Hutchinson-Gilford progeria syndrome. Nature 423(6937): 293-298.

104. Snowdon DA, Kane RL, Beeson WL, Burke GL, Sprafka JM, et al. (1989) Is early natural menopause a biologic marker of health and aging? Am J Public Health 79(6): 709-714.

105. Orgel LE (1963) The maintenance of the accuracy of protein synthesis and its relevance to ageing. Proc Natl Acad Sci USA 49(4): 517-521.

106. Ehrenberg L, von Ehrenstein G, Hedgran A (1957) Gonad temperature and spontaneous mutation rate in man. Nature 180(4599): 1433-1434.

107. Torrellas G, Maciá E (2012) Twist-radial normal mode analysis in double-stranded DNA chains. Phys Lett A 376(45): 3407-3410.

108. Cooper WG (1979) Proton transitions in hydrogen bonds of DNA. A first order perturbation model. Int J Quantum Chem Quantum Biol Symp 6(S6): 171-188.

109. Gillespie JH (2004) Population Genetics: A Concise Guide. The Johns Hopkins University Press.

110. Lynch M (2010) Rate, molecular spectrum, and consequences of human mutation. Proc Natl Acad Sci USA 107(3): 961-968.

111. Yartsev MM (2017) The emperor's new wardrobe: Rebalancing diversity animal models in neuroscience research. Science 358(6362): 466-469.

112. Carlén M (2017) What constitutes the prefrontal cortex? Science 358(6362): 478-482.

113. Buzsáki B, Llinás R (2017) Space and time in the brain. Science 358(6362): 482-485.

114. Timofeeff-Ressovsky NW, Zimmer KG, Delbrück M (1935) Über die Natur der Genmutation und der Genstruktur. Nachr Ges Wiss Göttingen 1(13): 190-245.

115. Schrödinger E (1944) What is Life? Cambridge University Press, Cambridge.

116. Löwdin PO (1963) Proton tunneling in DNA and its biological implications. Rev Mod Phys 35(3):724-732.

117. Löwdin PO (1965) Quantum genetics and the aperiodic solid: Some aspects on the biological problems of heredity, mutations, aging and tumors in view of the quantum theory of the DNA molecule. Adv Quantum Chem 2: 213-359.

118. Baltz RH, Bingham PM, Drake JW (1976) Heat mutagenesis in bacteriophage T4: The transition pathway. Proc Natl Acad Sci USA 73(4): 1269-1273.

119. Bingham PM, Baltz RH, Ripley LS, Drake JW (1976) Heat mutagenesis in bacteriophage T4: The transversion pathway. Proc Natl Acad Sci USA 73(11): 4159-4163.

120. Cooper WG, Kouri DJ (1972) N-particle noninteracting Green's function. J Math Phys 13: 809-812.

121. Kadenbach B, Munscher C, Frank V, Muller-Hocker J, Napiwotzki J (1995) Human aging is associated with stochastic somatic mutations of mitochondrial DNA. Mutation Res 338(1-6): 161-172.